IPP-Report

Max-Planck-Institut für Plasmaphysik

Reichbauer, T.

Assessment of Nitrogen Enrichment in Plasma Discharges cooled by Nitrogen Gas Puffing

IPP 2018-12
Juni 2018


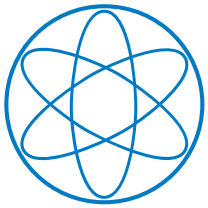


Master Thesis in Physics at
Technische Universität München

Assessment of Nitrogen Enrichment in Plasma Discharges cooled by Nitrogen Gas Puffing

presented by

Thomas Reichbauer

Garching, 24.04.2018

First Promoter: Prof. U. Stroth

Second Promoter: Prof. P. Feulner

Supervisor: Dr. V. Rohde

Contents

Chapter 1

Introduction

Energy consumption in Europe was rising until 2008 to its maximum of about 3400 TWh, while the years afterwards consumption stayed at this high level [1]. But the fraction of fossil fuels which is around 40% in the energy production mix has to decrease in the next decades rapidly to fulfill the Agreement of Paris and keep the global warming of Earth lower than 2°C compared to the global temperature average before industrialization. Therefore CO_2 neutral energy production has to replace coal and oil power plants. Europeans place high efforts in producing energy out of renewable sources like wind, water and solar power. But wind and solar energy is dependent on weather fluctuations. To guarantee a steady and stable supply of power in the future further steps have to be made. One of these steps must be the research on nuclear fusion power plants, which would provide huge amount of the base load energy which is needed in the future.

1.1 Nuclear Fusion as a Power Source

In fusion power plants it is tried to reproduce the nuclear processes of stars. These fusion power plants would produce electricity CO_2 neutral and compared to nuclear fission power plants it does not produce long-lasting nuclear waste. Additionally the fuel needed for operation is available and easily accessible.

1.1.1 Important Fusion Reactions

In the Sun, the main production of energy is produced by the so called proton-proton-chain reactions. The most dominant reaction chain is branch I which can be seen in figure 1.1. It fuses four protons to a helium nucleus, two positrons, two electron neutrinos and two gamma rays, see reaction equation 1.1.

$$4\,{}^{1}_{1}\mathrm{H} \rightarrow {}^{4}_{2}\mathrm{He} + 2\mathrm{e}^{+} + 2\nu_{\mathrm{e}} + 2\gamma + 26.7\mathrm{MeV} \tag{1.1}$$

The overall reaction rate of the pp-chain is very small [2] because of the small weak interaction cross section for the process ${}^{1}_{1}\mathrm{H} + {}^{1}_{1}\mathrm{H} \rightarrow {}^{2}_{1}\mathrm{D} + \mathrm{e}^{+} + \nu_{\mathrm{e}}$. There-

fore this reaction chain would lead to insufficiently high reaction rates in a planned commercial power plant.

Instead of the pp-chain typically another reaction is used, which does not include the weak interaction. The reaction rate of the fusion process 1.2 is much higher compared to other possible fusion processes [4].

$$ {}^{2}_{1}\mathrm{D} + {}^{3}_{1}\mathrm{T} \rightarrow {}^{5}_{2}\mathrm{He}^{\star} \rightarrow {}^{4}_{2}\mathrm{He} + {}^{1}_{0}\mathrm{n} + 17.6\mathrm{MeV} \tag{1.2} $$

In the favored reaction two isotopes of hydrogen are used, deuterium (D) and tritium (T). If the particles can overcome the Coulomb barrier it's energetically favorable for them to create a new particle. Because the generated isotope of helium ($^{5}_{2}\mathrm{He}^{\star}$) is decaying instantaneously ($\mathrm{T}_{1/2} \approx 7.62 \cdot 10^{-22}$ s) the end products are one helium nucleus ($^{4}_{2}\mathrm{He}$) and one neutron. The energy which is produced is stored in the kinetic energy of the end products.

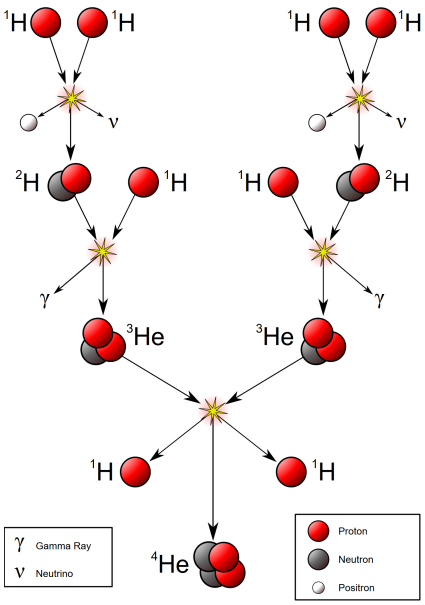

FIGURE 1.1: The proton-proton I branch [3]

1.1.2 Lawson Criterion

To overcome the Coulomb barrier high velocities of the particles ($\hat{=}$ high temperature of the gas/plasma) are necessary. By heating up the gas, particles become ionized and a plasma, a mixture of ionized atoms and free electrons, is created. A high temperature is a critical parameter for high reaction rates. The plasma needs to be heated up to about 100 million K. Additionally high particle densities should be reached to increase the number of collisions between the particles. But also the confinement time of the stored energy in the plasma is an important factor.
These three parameters are used in the Lawson criterion, which states that the triple product of temperature, density and energy confinement time has to be higher than a specific constant to achieve an ignition of the plasma [5]. This means that the heating of the plasma by the kinetic energies of the fusion products is sufficiently high to maintain the temperature of the plasma against all losses without external power input.

$$ T_e n_e \tau_E \geq 3 \cdot 10^{21} \, \frac{\mathrm{s} \cdot \mathrm{keV}}{\mathrm{m}^3} \tag{1.3} $$

1.2 Magnetic Confinement and Divertor Setup

To achieve such high values of the triple product magnetic confinement seems to be promising. The ionized particles can follow the magnetic field force freely. Particles with a vertical velocity component gyrate around the magnetic field line because of the Lorentz force. Therefore they are confined with help of magnetic fields.
For the confinement toroidal devices are used, i.e. tokamaks; see a schematic sketch in figure 1.2. To produce the magnetic field toroidal field coils are used. Because this pure toroidal magnetic field does not lead to a sufficient confinement an additional poloidal field is needed. This is produced by a plasma current. To establish this current a OH-transformer (ohmic heating) in the center of the torus can be used which induces it. The superposition of the toroidal and poloidal magnetic field leads then to good confinement conditions.
Additional coils are used to elongate the shape of the magnetic flux surfaces or have the possibility of controlling the plasma during discharges.

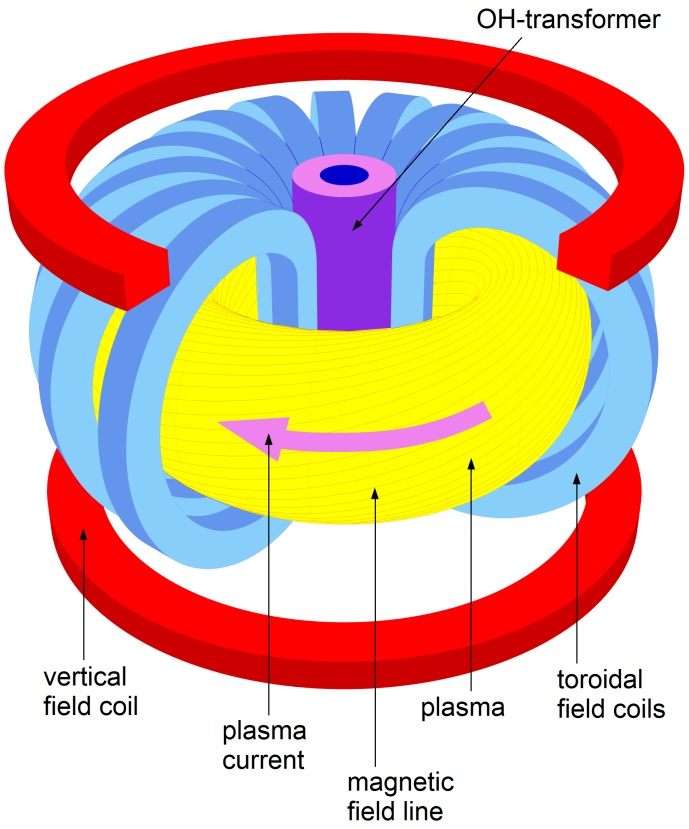

FIGURE 1.2: Basic structure of a tokamak (edited from [6])

The equilibrium condition for the plasma is described by equation 1.4. The force which is created by gradient of the pressure has to be counteracted by

the cross product of the plasma current and the created magnetic field.

$$\nabla \vec{p} = \vec{j} \times \vec{B} \tag{1.4}$$

Ionized particles have to move on the so called flux surfaces as long as there are no collisions. In the center of a toroidal device these surfaces are closed and the particles are trapped, i.e. confined (see red lines in the sketch below). The last closed flux surface is called separatrix. This is highlighted with a poloidal cross section, see sketch 1.3, where the separatrix is marked by a blue line. Outside of the separatrix the flux lines aren't closed anymore and ionized, energetic particles move to the plasma facing components (PFCs).

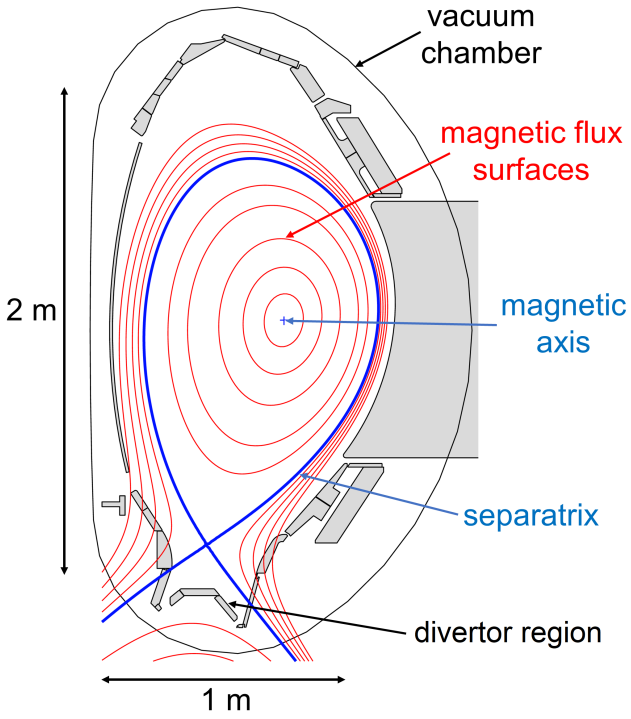

FIGURE 1.3: Poloidal cross section of the ASDEX Upgrade tokamak with flux surfaces (red) and highlighted separatrix (blue).

Nowadays in tokamaks a so called divertor is used to remove impurities efficiently from the plasma. It consists of a special magnetic configuration which can be seen in figure 1.3 and structural components here installed in the bottom part of the chamber. Ions which are outside of the separatrix will follow the magnetic field lines into the divertor regions and hit the PFCs. They become neutralized and can be removed by the pumping system. This leads to high particle fluxes during a discharge, especially during high heating phases and disruptions. Heat loads can reach up to 100 $\frac{\mathrm{MW}}{\mathrm{m}^2}$, which can lead to damages of the divertor tiles like sputtering, melting etc..
To avoid damaging the divertor tiles it is necessary to cool down the divertor and/or the incoming plasma. The former one is achieved in ASDEX Upgrade

by water cooling pipes. The latter one can be achieved by impurity gases which are introduced to the plasma near the divertor region.

1.3 Cooling by Impurity Seeding

Because acceptable heat loads for materials used in the divertor region are around 5 $\frac{\mathrm{MW}}{\mathrm{m}^2}$ cooling the plasma before it reaches the divertor is necessary. This can be achieved by radiation cooling. Therefore neutral gases from gas valves near the divertor region are puffed into the plasma. Typical gases for seeding are nitrogen N_2 or noble gases like neon Ne, due to their medium Z number and the resulting desired emission line radiation at temperatures where deuterium does not radiate. When the impurities interact with the plasma in the scrape of layer (SOL) they become excited and ionized. By falling back to lower energy states the difference of energy is radiated away and therefore the temperature in the SOL is decreased.
Additionally it shows that nitrogen seeding is not only reducing the heat flux onto the divertor but also improves the confinement of the plasma [7]. However besides the beneficial cooling nitrogen is also interacting with plasma facing components by sputtering the surface, ion implantation or chemical deposition like formation of WN_x or BeN [8]. This results in a build-up of nitrogen content.
Additionally, nitrogen is chemical active in a hydrogen environment which leads to formation of ammonia (NH_3) [9, 10].
For future devices, e.g. ITER, this means that a part of the radioactive tritium is bound by nitrogen and can lead to an additional inventory of radioactive material in the vessel. Furthermore this bound tritium must be removed from the residual gas by a tritium plant. Therefore it is important to estimate the ammonia production in the vessel and the storage on plasma facing components (PFCs).
Important questions to solve are:

- How much of the puffed nitrogen is interacting with the plasma and therefore makes a contribution to radiation cooling?
- Is it possible to link this puffed/interacting nitrogen with the production of ammonia?

The density of impurities can't get characterized by divertor diagnostics. The defining parameter for the nitrogen content in the plasma used so far is the seeding rate. However in the case of N_2 it seems this is not sufficient. Build-up of nitrogen wall inventory affects the N content in the plasma [11].

Chapter 2

Experimental Basics

The experimental data used in this work was obtained at the tokamak ASDEX Upgrade. In this chapter ASDEX Upgrade and important diagnostics for this thesis will be introduced.

2.1 ASDEX Upgrade

ASDEX Upgrade (**A**xial **S**ymmetric **D**ivertor **EX**periment) is operated at the Max-Planck-Institute of Plasma Physics (IPP) in Garching since 1991. Common technical parameters of the vessel and plasma experiments can be seen in table 2.1, where maximum values are given in brackets. The divertor of ASDEX Upgrade was optimized several times since 1991. 2013 the actual divertor setup III was installed and is operated till now. The divertor is made out of full tungsten tiles while all other plasma facing components are coated with tungsten. ASDEX Upgrade uses pure deuterium, protium or helium as

Parameter	Value
Vessel volume	41.56 m^3
Plasma volume	14 m^3
Major radius	1.65 m
Minor radius	0.50 m
Magnetic field	2.5 T (3.9 T)
Plasma current	0.6 - 1.0 MA (1.4 MA)
Discharge duration	$\approx$ 10 s

Table 2.1: Important parameters for the tokamak ASDEX Upgrade [12]

working gases for the plasma so fusion processes are not the main focus.
It is also possible to have a look at the Lawson criterion for ASDEX Upgrade. One can use $\tau_E \approx 0.1$ s, $n_e \approx 1 \cdot 10^{20}$ m^{-3} and $T_e \approx 3$ keV for this tokamak. This results in a triple product of about $T_e n_e \tau_E \approx 3 \cdot 10^{19}$ $\frac{s \cdot keV}{m^3}$, which is still

two orders of magnitude too small for a feasible high fusion rate if one would operate ASDEX Upgrade with a D-T mixture.
The upcoming sections give an overview of the main diagnostics which were used during this thesis and their principle of operation.

2.2 Pumping System

At ASDEX Upgrade cryo and turbo molecular pumps are used to achieve sufficiently low pressures and to remove the neutral gas from the plasma. The location of the cryo and turbo molecular pumps can be seen in figure 2.2. The cryo pump consists of a liquid helium LHe pump with a liquid nitrogen LN_2 shield. Because the boiling point of helium ($\approx$ 4.15 K) is smaller than the freezing point of deuterium ($\approx$ 18.7 K) LHe is used to trap deuterium onto the cryo pump while the LN_2 shield traps already other impurities like ammonia, methane and water. The turbo molecular pumps are located in segments 2, 3, 4, 5, 6, 8, 10, 12, 13, 15 and 16. Additional pumps are built in the NBI (Neutral Beam Injection) (titanium sublimation pumps) and diagnostic boxes (turbo molecular pumps). Their pumping speeds were determined in 2009 [13] with pure deuterium and can be seen in table 2.2. For calculations the

Pump	Pumping Speed [l/s]
	0.001 Pa $\leq p \leq$ 1 Pa
Turbo Molecular Pumps	$16100 - 6131 \cdot p + 1835 \cdot p^2$
Cryo Pump	$115000 + 276600 \cdot p$
NBI Box 1	$28350 + 46230 \cdot p$
NBI Box 2	$24660 + 31450 \cdot p$
Diagnostics	≤ 500

Table 2.2: Pumping speeds determined with deuterium at ASDEX Upgrade

pumping speeds of turbo molecular pumps in diagnostics can be neglected. During a discharge the pressure in the divertor is in the range of a few 0.1 Pa. In this pressure range the gas flow is in the transition area between molecular and laminar flow. Because of that the different residual gases are pumped with different speeds. But as deuterium is still the most abundant gas it will be assumed that the other components are carried with the deuterium flow and the given pumping speeds in table 2.2 are also applicable for all components of the residual gas. In a pure molecular flow of the gas this assumption would not hold.

2.3 Gas Inlet System

To insert gas for the plasma buildup the gas inlet system at ASDEX Upgrade is used. In total 19 piezo valves are used to puff in different kind of gases at different locations. By applying a voltage onto a piezo crystal it will deform and open the valve. An overview of their locations can be seen in figure 2.1. Gases can be puffed from various locations. At the region of the upper divertor

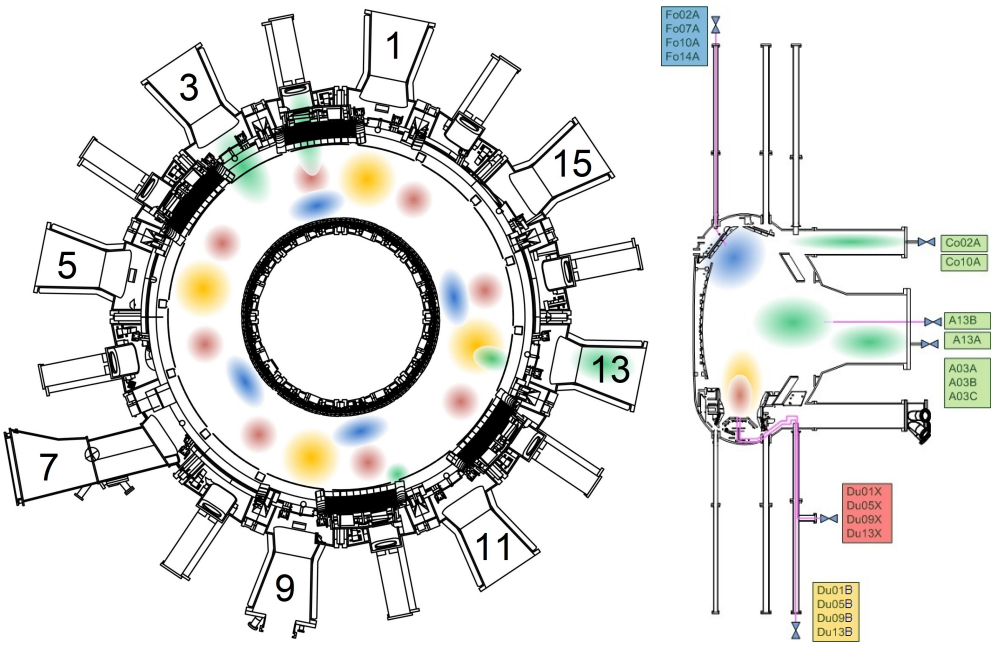

(a) Top view

(b) Cross section with sector numbers

FIGURE 2.1: Different positions of gas inlet system valves with highlighted puffing regions in a top view and cross section of ASDEX Upgrade

different valves can be used which are located in sector 2, 7, 10 and 14. At the midplane the valves are located in the Co or the A port and are available at sector 2, 3, 10 and 13. For puffing in gases in the lower divertor two different sets of valves can be used: the B and X setup. The B setup is puffing the gas at the specific sector while the X setup is splitting up again and is puffing then in the next 2 sectors nearby for a more symmetrical puffing. This means that the X valves are in total eight outlets, see top view of ASDEX Upgrade.
Commonly the Co02A valve is used to prefill the gas vessel with deuterium before the discharge. Then the DuxxB valves are used to feed the plasma with new deuterium.
For nitrogen seeding the DuxxX valves are used in different configurations.

2.4 Setup of Diagnostics

The main diagnostics to detect the different residual gases and its pressures are the mass spectrometers and the corresponding pressure gauges at the same location. In total 7 mass spectrometers are mounted in 4 different locations around the torus for detection of residual gases. In cross section 2.2 the exact measurement locations and their connections to the vessel can be seen.
Table 2.3 lists the exact positions of all used mass spectrometers and pressure

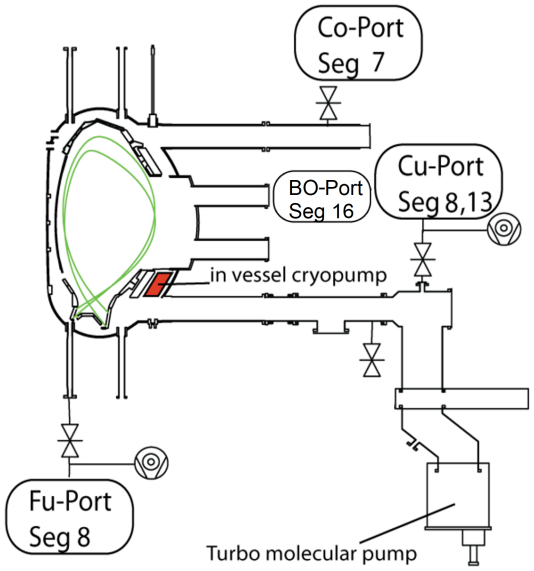

FIGURE 2.2: Positions of mass spectrometers and pressure gauges in a cross section of ASDEX Upgrade.

gauges. The given pressure gauges are mounted in front of the mass spectrometer boxes and therefore don't measure the additional pressure reduction which is necessary to have a low pressure for the mass spectrometers.

Position	Mass Spectrometer	Pressure Gauge (Vessel)
Inner Divertor (Seg. 8 Fu)	MKS HPQ3	2x MKS 627
Outer Divertor (Seg. 8 Cu)	MKS Microvision 2 Hiden Analytical HAL 201 RC	
Outer Divertor (Seg. 13 Cu)	MKS HPQ2, MKS HPQ3	MKS 690A, Granville Phillips 370
Midplane (Seg. 16 Bo)	Hiden Analytical HAL 201 RC	MKS 690A
Midplane (Seg. 7 Co)		MKS 690A, Granville Phillips 370

TABLE 2.3: Positions of pressure gauges and mass spectrometers

2.4.1 Pressure Gauges

To measure the pressure of the residual gas in ASDEX Upgrade different pressure gauges are installed around the vessel. The pressure range which has to be covered during measurement goes from $1 \cdot 10^{-8}$ Pa to 1 Pa. Therefore a coupling of a capacitance manometer and a more sensitive pressure gauge like a cold or hot cathode manometer is used in the same place.
For example in segment 13 the MKS 690A Baratron is combined with a Granville Phillips 370 which is a hot cathode manometer. The Baratron with a pressure range from $1.33 \cdot 10^{-3}$ to 1.33 Pa is a gas independent measurement. With a common error of 0.05% full scale it is additionally a very accurate gauge. As visible in figure 2.3a the capacitance manometers react to a pressure difference ΔP_v with a changed capacitance of the built in capacitor which is proportional to the pressure change. The reference pressure on the other side is maintained by an internal chemical getter pump. For low pressures a

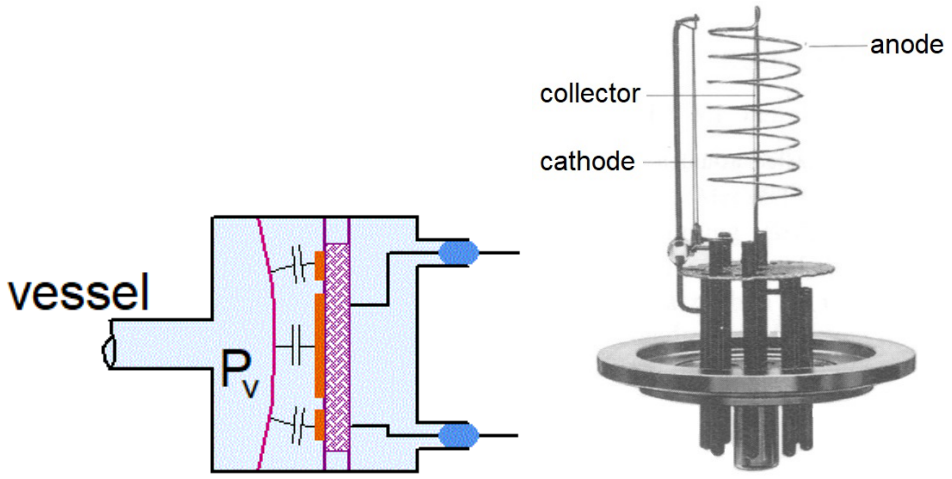

(a) Schematic of a Baratron [14]

(b) Schematic of a Bayard Alpert gauge

FIGURE 2.3: Schematic of different pressure gauges

hot cathode manometer (Bayard-Alpert) which is a Granville Phillips 370 is used (see sketch 2.3b). The pressure range is between $1 \cdot 10^{-8}$ Pa to 1 Pa with a error of around 5% of the measured pressure.
The cathode of the gauge is heated up, which ejects free electrons through thermionic emission. The electrons are accelerated to the ionization region with the help of an anode. If neutral gas particles are then colliding with the electrons the particles are ionized, e.g.

$$e^- + M \rightarrow 2e^- + M^+.$$

If the kinetic energy of the electrons is high enough it is also possible that particles can become ionized twice. Another possible effect is the dissociative

ionization. Molecules can be cracked which looks like

$$e^- + MX \rightarrow 2e^- + M^+ + X. \tag{2.1}$$

The ion current is then measured by the collector in the center of the gauge. Because the ionization efficiency for different gases is different this measurement is gas dependent.

2.4.2 Quadrupole Mass Spectrometer

In ASDEX Upgrade quadrupole mass spectrometers are used. These mass spectrometers mainly consist of three main parts.
First the residual gas has to be ionized. The ion source works the same way like the hot cathode manometers. By electron-particle collisions ionized or fragmented particles are created. Because the fragmentation is different for each ion source this has to be calibrated. Afterwards the ions get accelerated to the filter, the quadrupole.
The second main part is the quadrupole which acts as filter. It consists out of mainly 4 rods, which have alternating voltages. In figure 2.4 the voltage configuration can be seen, which is

$$U_1 = U + V\cos\omega t \quad \text{and} \tag{2.2}$$

$$U_2 = -U - V\cos\omega t. \tag{2.3}$$

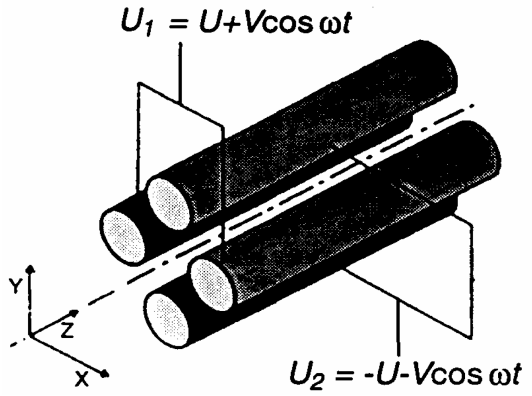

FIGURE 2.4: Voltage configuration of a quadrupole

If all four electrodes are superimposed it is possible to get the potential ϕ in the space between them:

$$\phi = (U + V\cos\omega t)\frac{x^2 - y^2}{r_0^2}, \tag{2.4}$$

where $2r_0$ is the distance between to rods on the same axis. We gain the equation of motions by using $\vec{F} = m\ddot{\vec{r}} = q\vec{E} = -q\nabla\phi$, where we can look at each coordinate respectively:

$$m\ddot{x} = -2q(U + V\cos\omega t)\frac{x}{r_0^2} \tag{2.5}$$

$$m\ddot{y} = 2q(U + V\cos\omega t)\frac{y}{r_0^2} \tag{2.6}$$

$$m\ddot{z} = 0 \tag{2.7}$$

where e is the elementary charge (assumed single ionized ions), m is the mass of the ions and r_0 is the inner radius of the quadrupole. It's already obvious that the velocity in z-direction is constant. With the parameters

$$a = \frac{8eU}{mr_0^2\omega^2}, \tag{2.8}$$

$$q = \frac{4eV}{mr_0^2\omega^2} \text{ and} \tag{2.9}$$

$$\xi = \frac{\omega t}{2} \tag{2.10}$$

it's possible to transform the differential equations to

$$x'' + (a + 2q\cos 2\xi)\cdot x = 0 \text{ and} \tag{2.11}$$

$$y'' = -(a + 2q\cos 2\xi)\cdot y = 0, \tag{2.12}$$

which leads to the normal form of the Mathieu's differential equation:

$$u'' = +(a - 2q\cos 2\xi)\cdot u = 0, \tag{2.13}$$

where $x'' = \frac{d^2x}{d\xi^2}$.
The solutions of the normal form of the Mathieu's differential equation [15] are

$$u = Ae^{\mu\xi}\sum_{n=-\infty}^{\infty} c_n e^{2in\xi} + Be^{-\mu\xi}\sum_{n=-\infty}^{\infty} c_n e^{-2in\xi} \tag{2.14}$$

with the characteristic coefficient μ, which is only dependent of a and q. Stable solutions exist if μ is purely imaginary. This can be better interpreted in an $a - q$ diagram, see figure 2.5. The operating line is only dependent on the voltages U and V by:

$$\frac{a}{q} = \frac{2U}{V} = \text{const.}. \tag{2.15}$$

Between q_1 and q_2 the operation line is inside the stable region. Therefore the mass resolution can be then determined by

$$\frac{4eV}{r_0^2\omega^2 q_1} = m_1 > m > m_2 = \frac{4eV}{r_0^2\omega^2 q_2}, \tag{2.16}$$

where the definition 2.9 was used. It can be seen that the mass resolution can be changed by changing the voltages U and V. By increasing the voltages successively it is possible to make a whole scan of different m/z ratios and therefore measure a total scan.
The third main part is the detector. The ions which passed the quadrupole

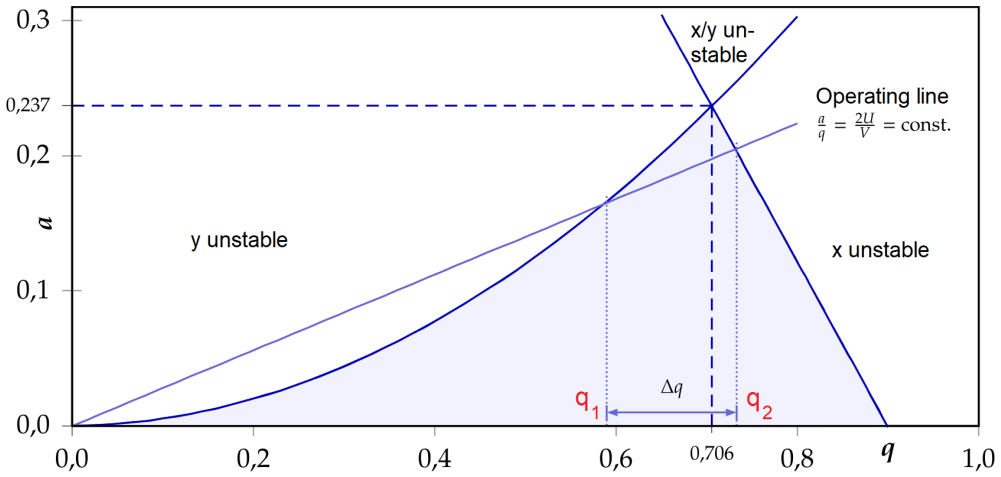

FIGURE 2.5: $a - q$ diagram of quadrupole

filter will be measured by a Faraday cup, which neutralizes the ions on the detector surface, which is at a specific potential, by electrons from the ground and measures the current which establishes due to the electron movement. Additionally some detectors have a secondary electron multiplier (SEM), which has a much higher sensitivity. The SEM is commonly used for pressures below 10^{-3} Pa.
Because the environment of the mass spectrometers is rough in a tokamak with high magnetic fields and high pressures arrangements were made. Because of the filter is susceptible to the high magnetic fields of the tokamak all devices are built into metal boxes built out of several single layers of iron which act as magnetic shielding because of the ferromagnetic behavior. Additionally high pressures in the mass spectrometers leads to collisions between ions during their way to the detector, which leads to non-linear effects in the measurement and is called *roll over*. Therefore all RGA boxes are differentially pumped. For measurements also at high pressures MKS HPQs are used which have very short quadrupoles and measure stable up to 0.1 Pa [16], while Hiden [17] and MKS MV [18] are working only stable till 10^{-2} Pa.

2.4.3 Measurement Setup for Mass Spectrometer

The RGAs are running in two different measurement modes. During a discharge, which is commonly around 10 seconds long, the pressure can rise up to 1 Pa and is dropping at the end of the discharge rapidly. Because of fast changes in pressure and gas mixture a high time resolution is needed. Therefore the so called 'peak-jump' mode is used. The analyzer is recording only at predefined m/z ratios which results in a time resolution of 0.5 seconds.
During the out-gassing phase of the shot, which usually is around 30 minutes long, the pressure drops to 10^{-4} Pa and lower. In this part of the discharge no big pressure drops occur and a high time resolution is not necessarily needed.

Therefore a so called 'profile' scan is done where whole spectra are recorded.

Setup during a Discharge

The peak-jump measurement is triggered roughly ten seconds before the shot starts. The measurement itself lasts 65 seconds for MKS devices and 60 or 90 seconds for Hiden Analytical devices. Additionally a second signal is recorded and acts as a synchronization signal for the beginning of the discharge itself. During the peak-jump mode only intensities at specific masses are measured. A typical list of recorded m/z ratios, used for detection of ammonia and other residual gases present during the shot is listed in table 2.4.

m/z ratio	Atom, molecule, fragmented molecule
14	Ammonia (N), Methane (CH_2, CD) and Nitrogen (N)
15	Ammonia (NH) and Methane (CH_3, CHD)
16	Ammonia (NH_2, ND), Methane (CH_4, CH_2D, CD_2), Water (O) and Oxygen (O)
17	Ammonia (NH_3, NHD), Methane (CH_3D, CHD_2) and Water (HO)
18	Ammonia (NH_2D, ND_2), Methane (CH_2D_2, CD_3) and Water (H_2O, DO)
19	Ammonia (NHD_2), Methane (CHD_3) and Water (HDO)
20	Ammonia (ND_3), Methane (CD_4), Water (D_2O) and Neon ($^{20}_{10}$Ne)
22	Neon ($^{22}_{10}$Ne)
23	Zero Signal
28	Nitrogen (N_2)
32	Oxygen (O_2)

Table 2.4: Standard peak-jump measurement during a shot.

After the predefined measurement time of the peak-jump mode the mass spectrometers switch then automatically back to the profile scan mode.

Setup between Discharges

Between two discharges whole spectra are recorded during the profile scan. The profile measures usually from $m/z = 1$ to $m/z = 50$ with a resolution of 0.06 and 0.12 amu. An example of such a spectrum can be seen in figure 3.3.

Settings Used

The optimization of the settings of the mass spectrometers was already done during the diploma thesis of D. Neuwirth [9]. The settings which are used for the divertor mass spectrometers can be seen in table 2.5.

Parameter	HPQI	HPQO	HPQO2	MV	HIDEN2
Electron energy [eV]	70	70	70	70	70
Emission current [mA]	0.39	0.39	0.39	1.0	1.0
Extraction potential [V]	-110	-110	-110	-112	-90
Ion energy [eV]	7.0	7.0	8.0	5.0	3.0

TABLE 2.5: Settings for the mass spectrometer heads

2.5 Calibration of Mass Spectrometer

To connect the measured intensity of the mass spectrometer with a real partial pressure of the gas it is important to know this calibration factor (CF). Hidden in this factor is for example the unknown ionization probability of the specific gas component in the ion source, the unknown efficiency of the detector and the transport of the gas from the vessel to the RGA.
For a more reliable detection of residual gas molecules like methane, ammonia and water it is important to know the probability of the fragmentation of the molecule in the ion source. Fragmentation of molecules (see equation 2.1) occur because the electron energies are much higher than the binding energies of hydrogen atoms.
Calibration is performed by letting in gas at known pressures measured by the pressure gauges. This can be linked to the measured intensities from the RGA which results in a calibration factor. This calibration factor allows to calculate the partial pressure of specific impurities in the vessel during operation.
During calibration the cryo pump was at room temperature. For each measurement setup the torus was evacuated and then all shutters were closed to the TPS (Torus Pump System) turbo molecular pumps (TMPs). Through piezo valves a small amount of gas was injected into the vessel and measurements were made for at least 3 minutes to have enough data points for a specific pressure. This was repeated up to 8 times to have measurements for a wide range of pressure. At the end the valves to the TMPs were opened and the torus was evacuated again.
This calibration procedure was done for different impurity gases like methane and nitrogen. Important to note is that this procedure is only useful for gases which are not sticking onto plasma facing components or ducts. Otherwise no stable pressure could be achieved and the pressure measurements could not be linked directly to the intensities of the different mass spectrometers. Ammonia is such a sticking molecule and therefore the described calibration procedure is not useful because of the sticking effect [9]. It takes up to half an hour to reach a stable pressure in the plasma vessel. Therefore another method was used to calibrate ammonia which will be described later in more detail (see section 3.3).

First of all an impurity gas was puffed in purely while measuring the intensities with the mass spectrometers. Usually this was done with pure deuterium

(D_2), nitrogen (N_2) and sometimes with methane (CH_4). Deuterium is not measured during operation but with the calibration of deuterium a check was done if the device works properly.
With the help of these data it is possible to calculate the different calibration factors which can be multiplied to assess the partial pressure of the gas out of the measured intensities and also to calculate the cracking patterns for the specific devices, which are very important because these can be significant different between the devices itself.
On the 23rd of October 2017 calibration of deuterium, nitrogen and methane for the MKS diagnostics was done. Additionally it was possible to gain a set of data for water during the evacuation at the beginning of the measurements. The raw detected intensities of deuterium, methane and nitrogen are shown in figure 2.6, 2.7 and 2.8 respectively. Additionally the total pressure measured by the baratron in the midplane in sector 7 is shown in all graphs as chocolate colored line.

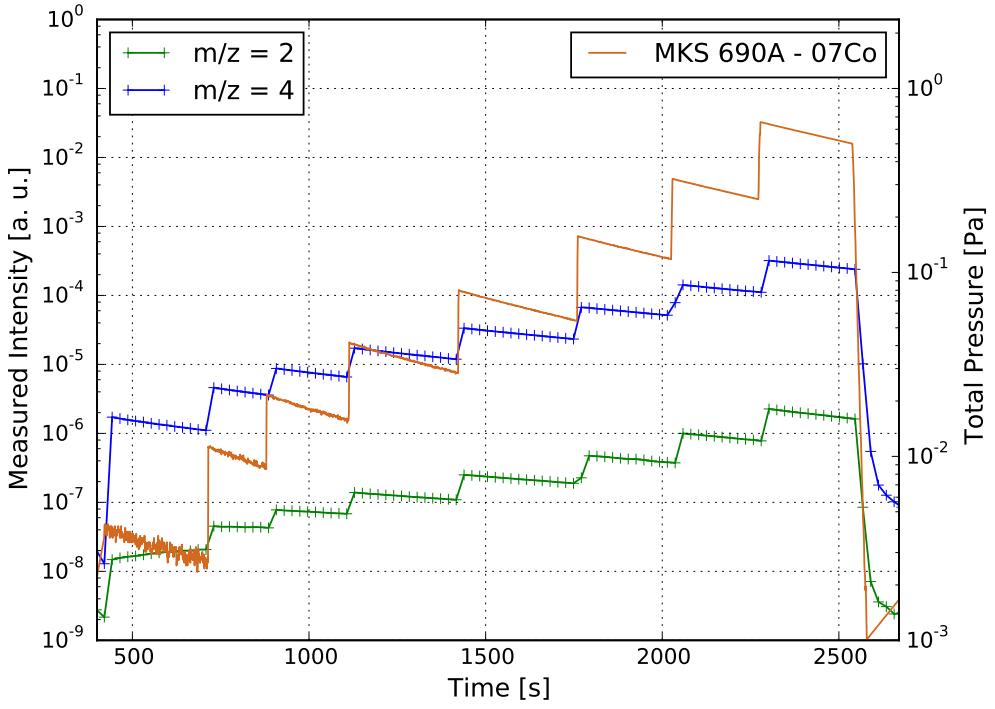

FIGURE 2.6: HPQI: Measured data during calibration with deuterium

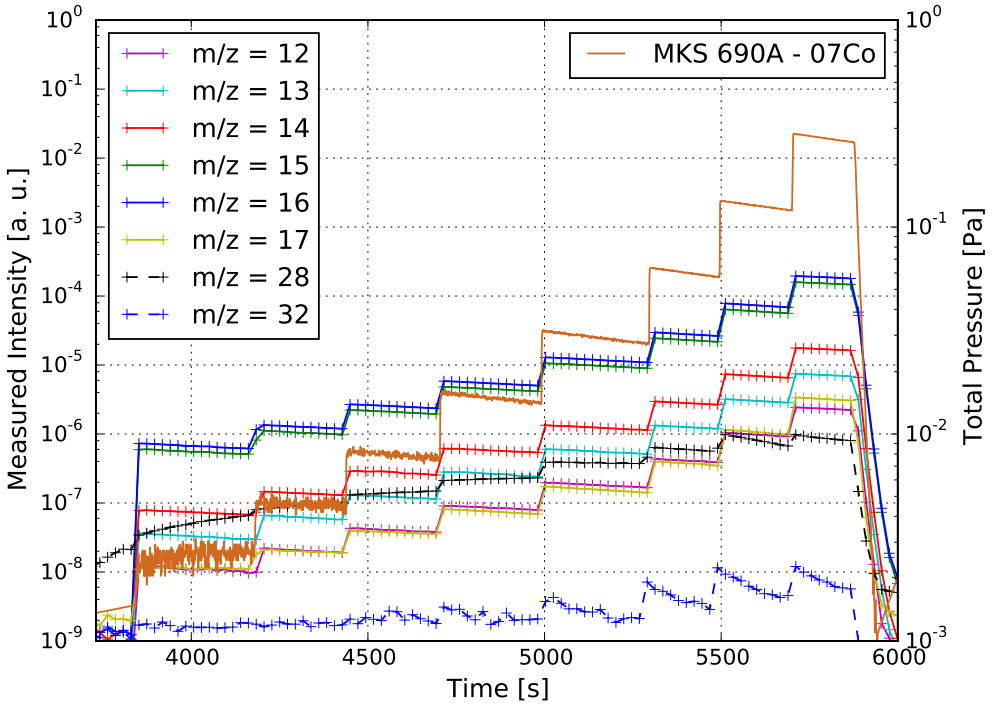

FIGURE 2.7: HPQI: Measured data during calibration with methane

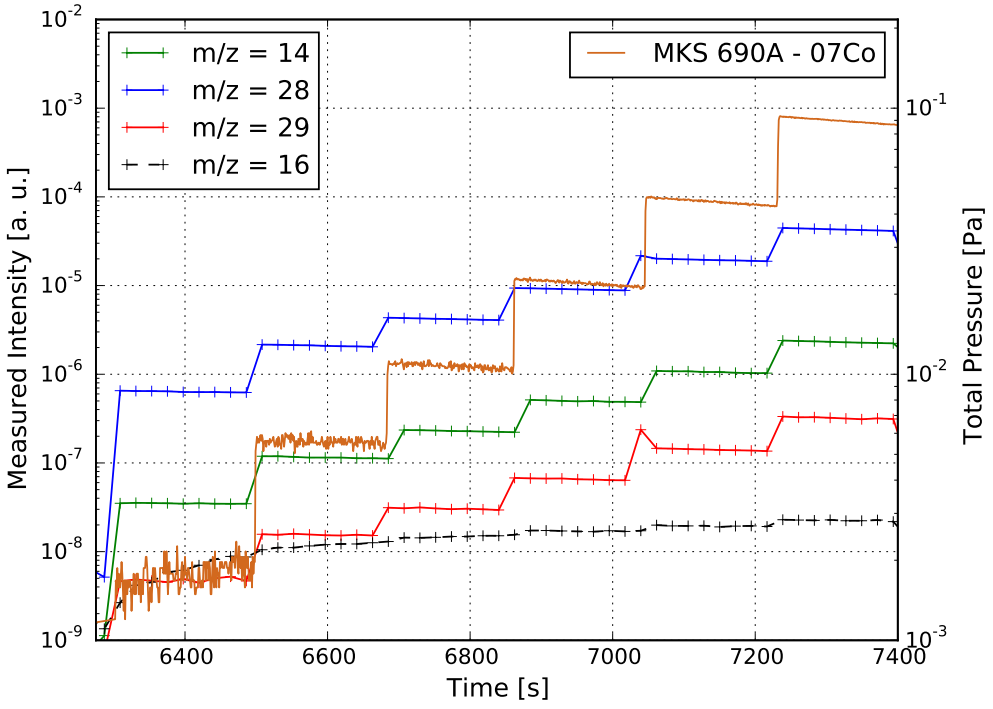

FIGURE 2.8: HPQI: Measured data during calibration with nitrogen

Calibration Factor

For the calculation of the instrument sensitivity the pressure measurement of baratron MKS690A in sector 07Co was used. The measured pressures in Pa could then be correlated to the measured intensities of the mass spectrometers. If the pressure is low ($\leq 10^{-3}$ Pa) the dependency should be linear, but if the pressure is higher collisions in the mass spectrometer play a role and the measurement is not linear anymore. Therefore in the linear and near-linear regime a quadratic function $f(p)$ with variables a, b and c was fitted, where p is the partial pressure.

$$I(p) = f(p) = ap^2 + bp + c \tag{2.17}$$

The calibration factor is connecting the measured intensity to the real measured (partial) pressure by the baratron. It is defined as

$$\frac{1}{CF(p)} = \frac{dI(p)}{dp} = \frac{df(p)}{dp} \tag{2.18}$$

which results in

$$CF(p) = \frac{1}{2ap + b}. \tag{2.19}$$

For deuterium m/z = 4, for methane m/z = 16 and for nitrogen m/z = 28 $f(p)$ was fitted. The raw data points and the fitted lines can be seen in figure 2.9. If the derivative of the pressure functions are calculated the correction factors

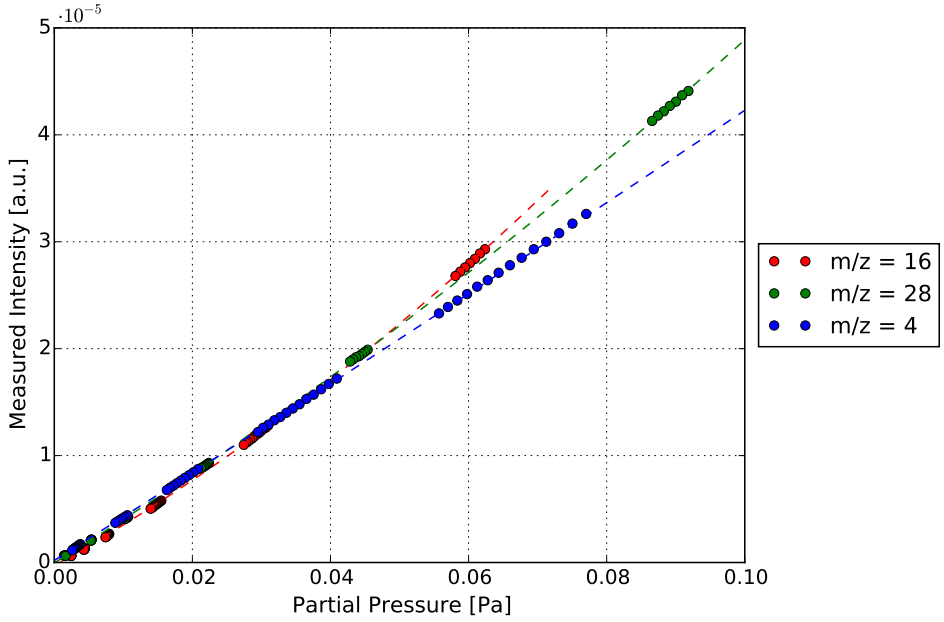

FIGURE 2.9: HPQI: Measured total pressure (MKS 690A - 07Co) of gases compared to its measured intensities at the main peak

are gained in dependency of the partial pressure of the gases. In figure 2.10

the dependencies can be seen. Even for high pressures the calibration factors for deuterium, nitrogen and methane stay constant, which indicates that for pressures up to 0.1 Pa non-linear effects play a minor role for HPQI.

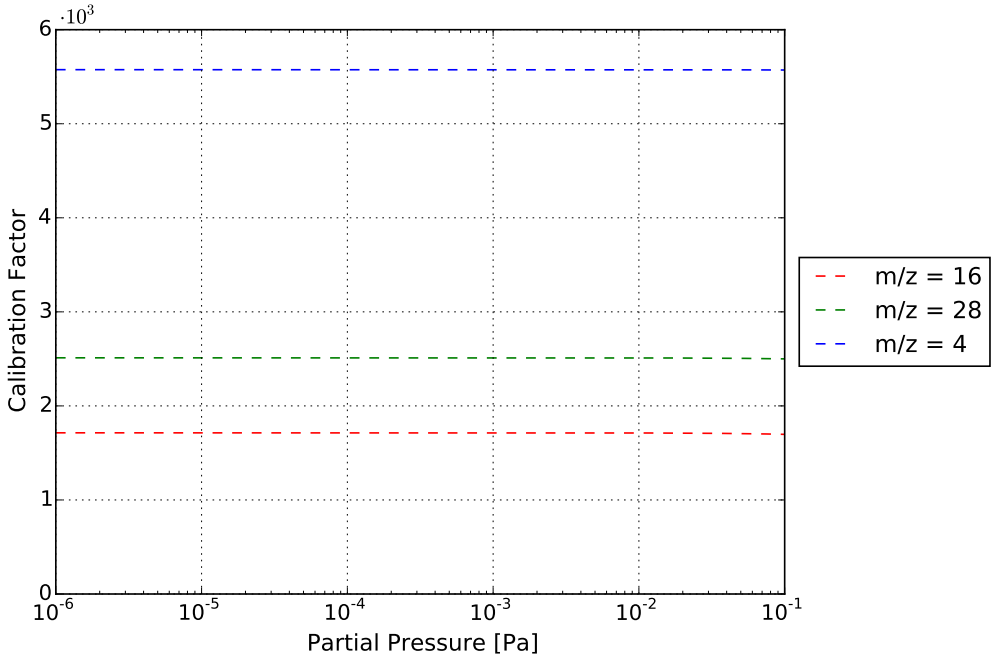

FIGURE 2.10: HPQI: Calculated Correction Factor in dependency of the partial pressure

Cracking Pattern

The binding energies of the hydrogen atoms in the molecules like methane, ammonia and water are about 4 to 5 eV [19] which is much lower than 70 eV. During the ionization in the ion source the molecule becomes excited and therefore can become dissociated. Because of that there's a probability of fragmenting/cracking the molecules in the ion source region of the mass spectrometer in reactions like 2.1. This is an equilibrium reaction but however because of low pressure inside of the mass spectrometers this can be neglected and it is assumed that if a fragmentation takes place in the ion source there is no recombination afterwards. Because of that methane is not only visible at $m/z = 16$ but also at m/z ratios of 12, 13, 14 and 15 (see figure 2.11). This leads to the fragmentation vector $\vec{p}$ which is normalized to the non fragmented m/z ratio of the molecule, for instance of methane and device HPQI 2.11 for low pressure we gain:

$$\vec{p}(\text{Methane, HPQI}) = (1, 0.83, 0.109, 0.05, 0.016)^{\mathrm{T}}. \tag{2.20}$$

The n'th element of the vector is then the probability of a n-1'th fragmentation of the molecule. The probability to fragment the methane molecule to CH_2

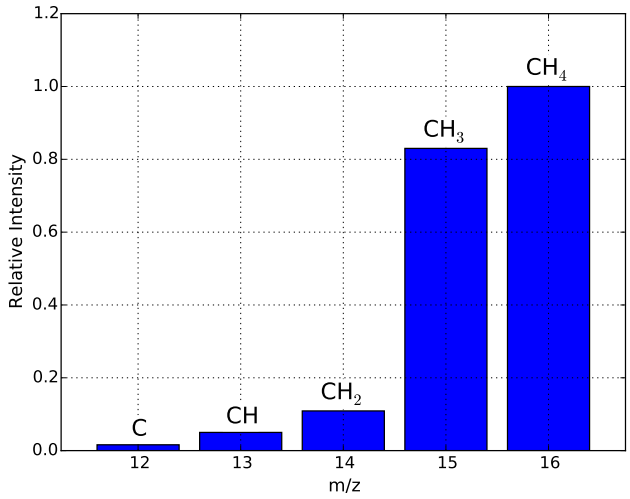

FIGURE 2.11: Fragmentation of the methane molecule leads to a measurement of CH_4 at m/z ratios with a specific relative intensity.

and H_2 is still 10.9%. Additionally the vector has the length x+1, where x is the number of hydrogen atoms in the molecule. Therefore the fragmentation vector of methane has a length of 5, while the fragmentation vector of ammonia has a length of 4.
If isotopically pure gases for calibrations are used a direct measurement of the fragmentation is possible. The fragmentation vector can be described by the calculated calibration factors for different m/z ratios which leads to the calculation of the n'th element of the fragmentation vector like

$$p_n = \frac{df_{m/z=N-n}}{df_{m/z=N}}, \tag{2.21}$$

where N is the mass number of the molecule and n is the number of fragmented hydrogen atoms, which can be between 0 and x (the total number of hydrogen atoms).
If this is then used on the measured data of methane we get a pressure dependent fragmentation vector, which can be described as constant for low pressures (see equation 2.20) for the mass spectrometer HPQI. For higher pressures a small decrease can be seen in figure 2.12.

As already mentioned above a main assumption was that no recombination of fragmented molecules is happening due to low pressures. If the pressure rises it is more probable that a recombination occurs and therefore the intensity of fragmented molecules should become smaller, which can be seen also in the results.

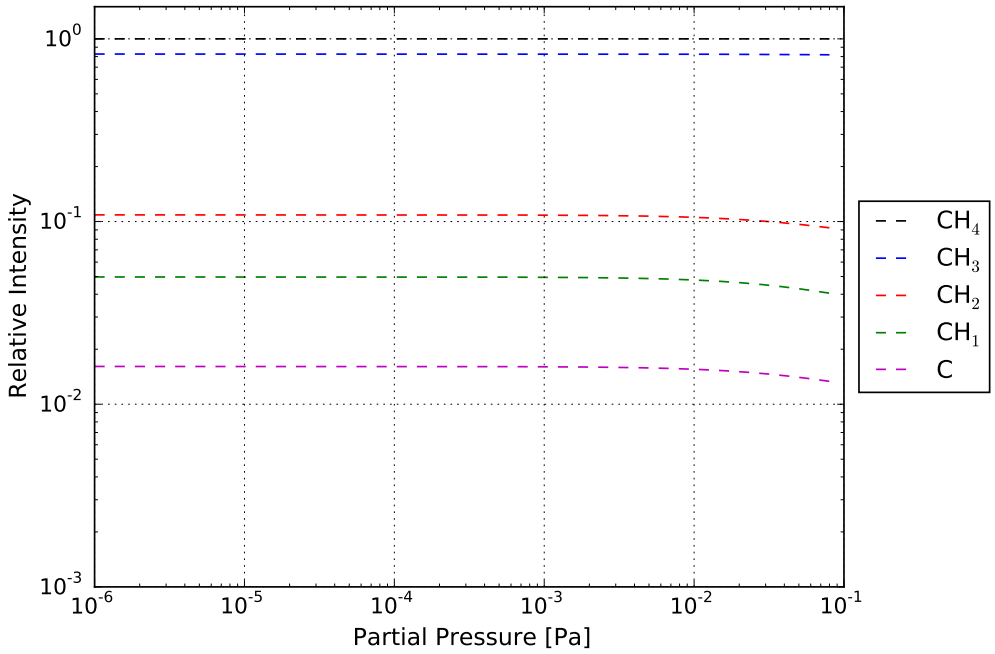

FIGURE 2.12: HPQI: Measured Fragmentation Vector for CH_4 in dependency of the partial pressure

In the previous calibration several assumptions were made:

- The background like nitrogen or oxygen do not disturb the fragmentation vector/cracking pattern calibration.
- Isotopes of the impurity atoms can be neglected, e.g. $^{13}_{6}C$ for methane.
- Molecules do not exchange hydrogen isotopes on wall components.

A main assumption is that impurities like nitrogen or oxygen which would affect $m/z = 14$ or 16 are negligible. Indeed this can be seen already in the raw data of methane (see figure 2.7), where the main impurities nitrogen ($m/z = 28$) and oxygen ($m/z = 32$) are commonly at least one order of magnitude lower and their fragmentation to N or O would be additionally one order lower. Furthermore no effect on the intensities at $m/z = 14$ respectively $m/z = 16$ is noticeable.
The occurrence of $^{13}_{6}C$ is approximately 1.1% and of $^{15}_{7}N$ is roughly 0.4%. The impact of the cracking pattern for methane and ammonia is therefore negligible.
Another assumption is that only molecules with protium are measured and no hydrogen isotope exchange takes place during calibration on the wall surfaces due to deuterium still stored on the walls after discharges.
By having a closer look to the ratio of $m/z = 17$ to $m/z = 16$ it is possible to see if the last two assumptions are valid. In figure 2.13 the ratio of both m/z

ratios can be seen. It stays more or less constant with a value of

$$\frac{m/z = 17}{m/z = 16} = 0.0148 \pm 0.0015. \tag{2.22}$$

Out of this it's possible to conclude that the rise of $m/z = 17$ is linked to

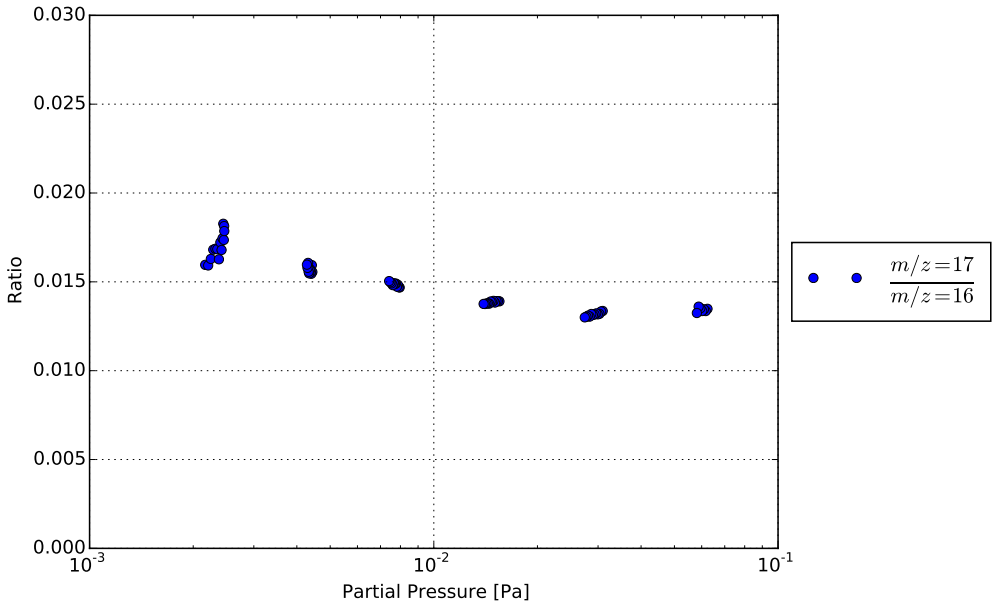

FIGURE 2.13: Assessment of influence of ${}^{13}_{6}\mathrm{C}$ onto measurements by comparison of $m/z = 17$ with $m/z = 16$ for methane

methane which is inside the vessel. Out of the 1.5% of molecules which have a m/z ratio of 17 already 1.1% are methane molecules with a ${}^{13}_{6}\mathrm{C}$. The difference (0.4%) should be then atoms which could exchange a protium with a stored deuterium atom on the wall. Overall these 1.5% are not disturbing the cracking pattern significantly.

Chapter 3

Data Evaluation

3.1 Model for Cracking Pattern

During plasma discharges in ASDEX Upgrade a mixture out of protium and deuterium is present. Deuterium is used as plasma fuel while protium comes from impurity sources like water from a leak. Because both are acting chemically identically ammonia, methane and water can create bonds to both varieties of hydrogen equally. Now methane does not only appear as CH_4 but additionally 4 different molecules exist: CH_3D, CH_2D_2, CHD_3 and CD_4. Each molecule has a separate fragmentation vector. This leads to 13 unknown variables (the partial pressures) for each possible molecule of ammonia (4), methane (5), water (3) and nitrogen (1).
To reduce the number of free parameters the model of Price and Iglesia [20] was applied. With the assumptions, that the fragmentation vector of each isotopologue is the same and the probability of each mixed molecule is statistical weighted, the probability for each molecule can be described with the Binomial distribution

$$w_z = W(XH_yD_z) = R^y \cdot (1-R)^z \cdot \frac{(y+z)!}{y!z!}, \tag{3.1}$$

where R is

$$R = \frac{N_H}{N_H + N_D}. \tag{3.2}$$

The factor R can take a value between 0 and 1 and is aligned with the so called HD ratio which is defined by

$$\text{HD ratio} = \frac{N_H}{N_D} = \frac{R}{1-R}. \tag{3.3}$$

With the help of the model the open parameters reduce from 13 to 7: the partial pressure for each molecule and the R value for ammonia, methane and water.
Now it is possible to describe the formation of a methane molecule at a specific m/z ratio, e.g. $m/z = 18$ for all different types of starting molecules. It leads

to three possible reactions,

$$CD_4 + e^- \rightarrow CD_3^+ + D + 2e^-, \tag{3.4}$$
$$CHD_3 + e^- \rightarrow CD_3^+ + H + 2e^-, \tag{3.5}$$
$$CH_2D_2 + e^- \rightarrow CH_2D_2^+ + 2e^-, \tag{3.6}$$

where the first two reactions refer to a fragmentation of the molecule and the last reaction did not fragment the molecule. The probabilities for such reactions are described by equation 3.1. Therefore the first reaction has the probability w_4. The second one has the probability $w_3/4$. The factor $1/4$ handles the fact that the last protium in the molecule has to be hit. By multiplying these specific occurrence probabilities of the reactions with the probability of the specific fragmentation that leads then to the real measured intensity at a specific m/z ratio. In total the cracking pattern is then calculated by the probability of each molecule at a specific R value and the relating fragmentation vector of the molecule

$$\overrightarrow{CP}(R) = \mathcal{A}(R) \cdot \vec{p}, \tag{3.7}$$

where $\mathcal{A}$ is a probability matrix. The full matrices for all three molecules can be seen in appendix A.
Now it is also possible to have a look on the HD ratio or R dependent cracking pattern. By using the before described probability matrix $\mathcal{A}$ and the calibrated fragmentation vector $\vec{p}$ of the device HPQI it is possible to calculate the cracking pattern with equation 3.7. The result of the calculation for methane can be seen in figure 3.1.

In this model it is assumed that the fragmentation probability in the ion source of hydrogen and deuterium to its impurity atom are the same. D. H. Lenz and WM. C. Conner showed that this is not the case [21]. In a detailed analysis of the different bindings C-H and C-D it was found that the difference is described by a factor between 1.1 and 1.25. The arising cracking patterns are still roughly the same with an error of around 10%.

3.2 Fitting Routine

Once the cracking patterns of methane, ammonia and water are determined (or taken of a database) it is possible to gain the partial pressures of these gases. By fitting the above model to the measurement the free parameters are optimized.
For each measurement cycle, around 50 during peak mode and around 40 in the analog mode an automatized evaluation package for the measured data is necessary. Therefore a minimization routine, described by F. Reimold in 2008 and 2009 [22] (in IDL) and a similar approach by A. Drenik [23] was used to calculate partial pressures of the main residual gases by minimization of a

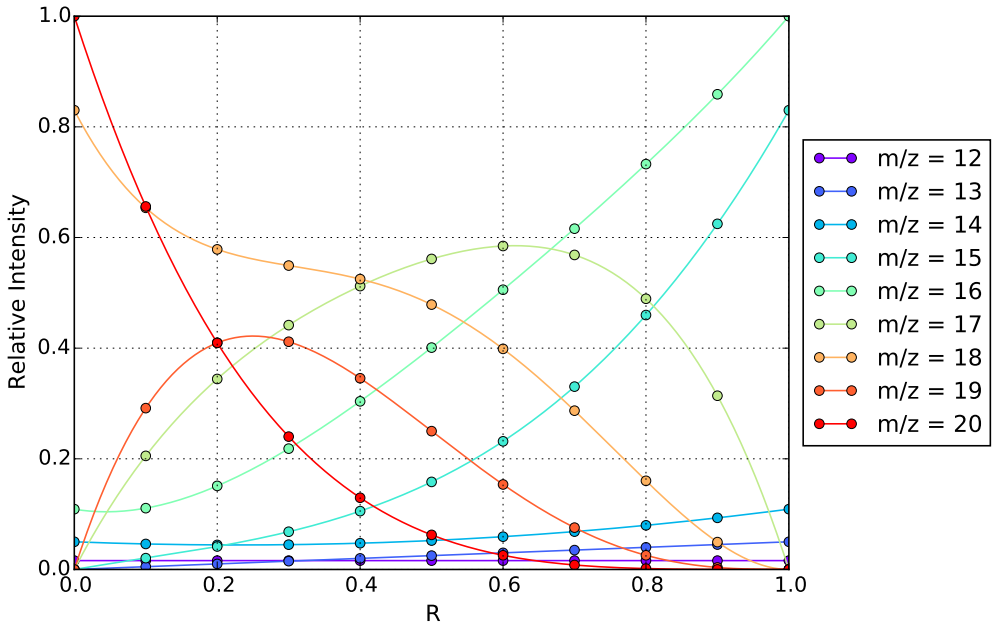

FIGURE 3.1: Calculated Cracking Pattern of CH_4 in dependency of R

residual S (see equation 3.8) and R.

$$\begin{aligned} S = (&\gamma_{\text{Ammonia}} \cdot p.p._{\text{Ammonia}} \cdot \mathcal{A}_{\text{Ammonia}}(R_{\text{Ammonia}}) \cdot \vec{p}_{\text{Ammonia}} \\ &+ \gamma_{\text{Methane}} \cdot p.p._{\text{Methane}} \cdot \mathcal{A}_{\text{Methane}}(R_{\text{Methane}}) \cdot \vec{p}_{\text{Methane}} \\ &+ \gamma_{\text{Water}} \cdot p.p._{\text{Water}} \cdot \mathcal{A}_{\text{Water}}(R_{\text{Water}}) \cdot \vec{p}_{\text{Water}} \\ &+ p.p._{\text{Nitrogen}} \cdot \vec{p}_{\text{Nitrogen}} - \vec{I})^2 \end{aligned} \tag{3.8}$$

γ_i is the relative intensity, $p.p._i$ is the partial pressure and $\mathcal{A}_i \cdot \vec{p_i}$ is the cracking pattern of each molecule. The minimization procedure has 7 unknown variables: the partial pressures of each molecule and the time dependent R value, which is located in the matrix $\mathcal{A}$.
The partial pressures of the routine results are still in arbitrary units, as the input data. Therefore some extensions to the original code were made:

- Introduction of the calibration factors to gain partial pressures in Pa.
- Calculation of the total number of molecules.

In total the basic data evaluation procedure can be seen in flow chart 3.2. First the considered molecules and possible boundary conditions on R have to be handed over to the fitting routine. Specific m/z ratios can be disregarded by the fitting routine to take the influence of other dominating impurities into account. An example would be $m/z = 14$ which is mixed by highly fragmented molecules of ammonia, methane and water and fragmented nitrogen. But during seeded discharges nitrogen is dominating and therefore the fitting of the other impurity gases is affected. To correct the raw data of the measurements

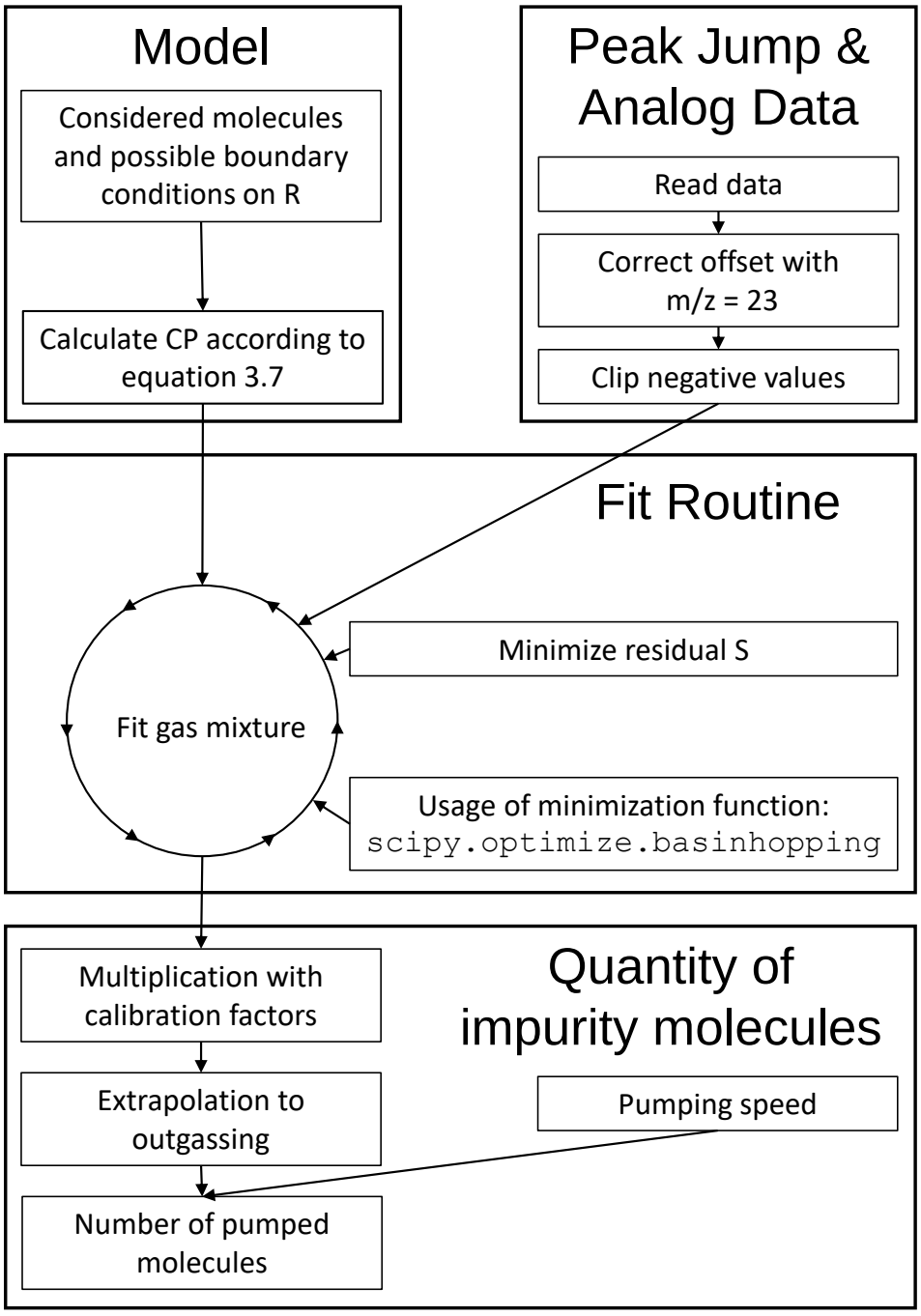

FIGURE 3.2: Flow chart of the fitting routine by Aleksander Drenik with extensions for the thesis.

a intensity at a specific m/z ratio is used. In typical vacuum system conditions $m/z = 5$ might be a good choice. Low concentrations of He in air would not disturb this measurement. But this is not the case for ASDEX Upgrade. Because deuterium is used as fuel in ASDEX Upgrade the intensity at $m/z = 4$

is extremely high. This is influencing the measurement at $m/z = 5$ significantly. Therefore the offset measurement is done at $m/z = 23$. As shown in figure 3.3 around $m/z = 23$ only noise is visible, while next to $m/z = 5$ the high intensity of deuterium can be seen. In the spectrum the clear impact of deuterium at $m/z = 4$ is visible which is the most abundant gas. Between $m/z = 14$ and 20 the residual gases of ammonia, methane and water can be seen. Ratio $m/z = 14$ is dominated by nitrogen, which has the main peak at $m/z = 28$. The last clear peak is visible at $m/z = 44$ which corresponds to CO_2. Because the magnetic field or electromagnetic interferences can lead to

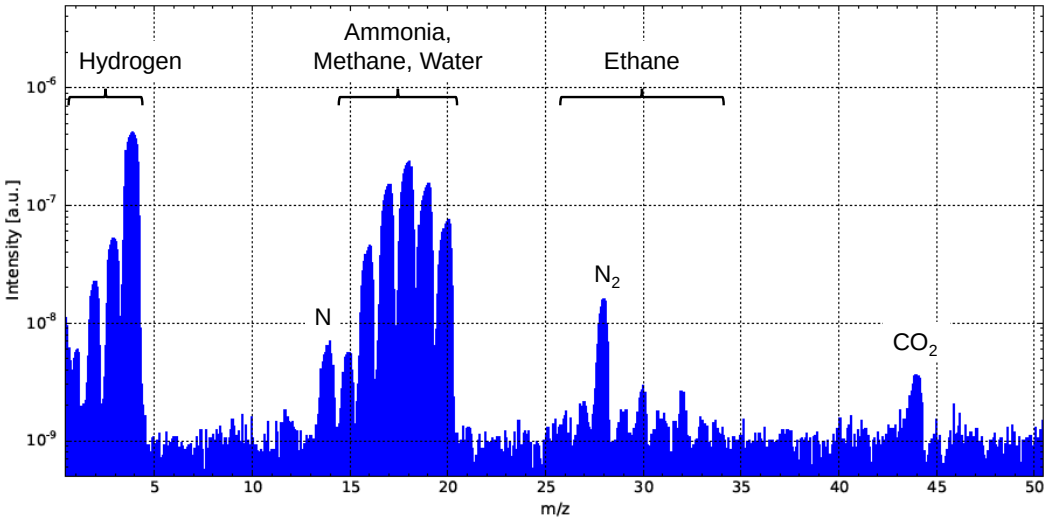

FIGURE 3.3: First raw fully measured spectrum after discharge 34266 for HPQI around 50 seconds after the discharge

a high background, the raw data of peak mode and analog mode are first corrected by this signal. Therefore the intensity of $m/z = 23$ is subtracted from all other measurements. Afterwards the resulting small negative intensities are clipped and set to 0. As an example the corrected raw data during discharge 34266 can be seen in figure 3.4. Table 3.1 sums up the different phases before, during and after shot 34266. During the discharge a high time resolution is required, therefore peak jump mode is used, while after the discharge this is not necessary and the analog mode is used. The first 19 measurement steps are prior the discharge. The second part highlights the discharge itself. The intensities are rising significantly, especially for $m/z = 28$ which indicates the high puffing of nitrogen during the shot. Also the impurity m/z ratios are rising significantly during the shot, especially $m/z = 17$ - 20. This indicates that deuterated impurity gases are formed. The third and fourth section of the plot illustrates the after-discharge measurements, while the third one is still recorded in peak mode and the last one is recorded by analog mode. During these two sections the intensities are rapidly dropping. The kink in between both measurements is due to the different time scales of both recording types, as indicated by the time axis at the top of the figure, and is no non-physical

Phase	Measurement Steps	Timespan [s]	Time Resolution of HPQI [s]
Peak-jump	0 - 52	-11 - 20	0.5
Analog scan	53 - 97	20 - 1500	50
Prior discharge	0 - 19	-11 - 0	0.5
Discharge	20 - 35	0 - 9	0.5
After discharge	36 - 97	9 - 1400	0.5 or 50

TABLE 3.1: Summary of different phases during discharge 34266 for HPQI

behavior.
The noise level during the peak mode is much larger because a better time resolution is required, in contrast to the analog mode where the measurement time per scan is bigger. This difference can be seen when the pre-discharge phase (already peak mode) is compared with the end of the analog mode.
The corrected data from figure 3.4 is handed over to the fitting routine which minimizes equation 3.8 by varying the partial pressure and R inside the given boundary settings of each molecule. The least squared sum is found by using the `scipy.optimize.basinhopping` function of the `scipy` package in `Python`. The feedback of the fitting routine is still in the same units as the input data i.e. the partial pressure of the impurities are still given in arbitrary units. By applying the calibration factors for all impurities (see appendix C), which were gained during the calibration procedure, the partial pressures of the different impurity residual gases are calculated in Pa.
For the minimization procedure the four main impurities during a nitrogen seeded discharge are considered: the seeding gas nitrogen, ammonia, methane and water. The partial pressures of the impurities for discharge 34266 can be seen in figure 3.5. Prior the discharge in the RGA signal water from residual leaks can be seen, while other m/z ratios are near the noise level, therefore the data in this interval is not useful. During the discharge the huge amount of nitrogen of the puffing is visible in the residual gas. This follows a clear build up of ammonia. Methane and water are still present but their part in the residual gas is much smaller than ammonia. After the discharge methane drops instantly back to very small background values. Nitrogen is dropping rapidly while ammonia needs a much longer time to decrease, because of the sticking effect of the molecule on plasma facing components [9]. Water is decreasing to a background level which can be assumed to be around $2 \cdot 10^{-5}$ Pa for HPQI.
For the three main impurities which are still visible during the analog scan mode an exponential fit was used for a better calculation of integrated intensity values and as extrapolation to the out-gassing.

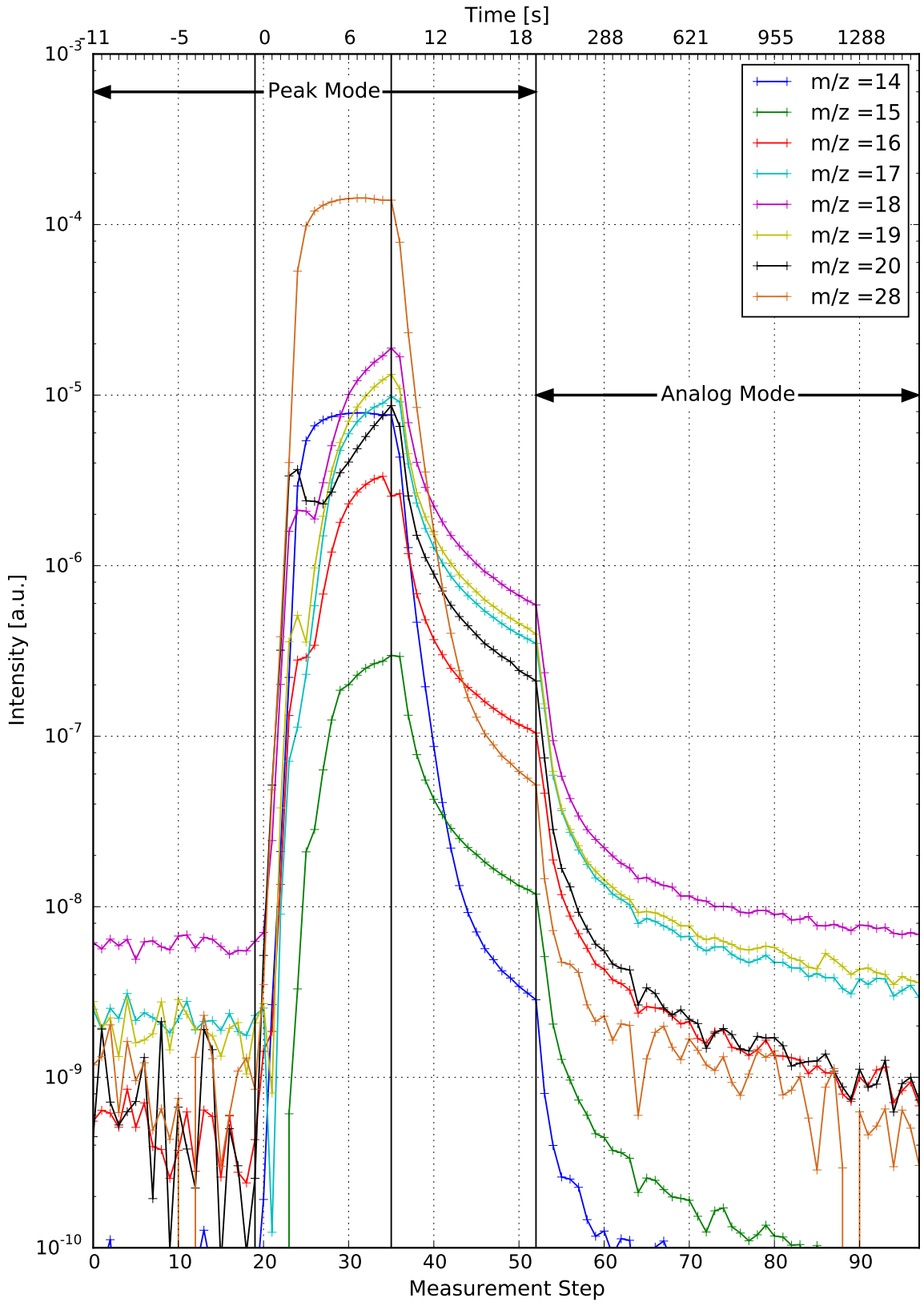

FIGURE 3.4: Corrected raw data of discharge 34266 and device HPQI

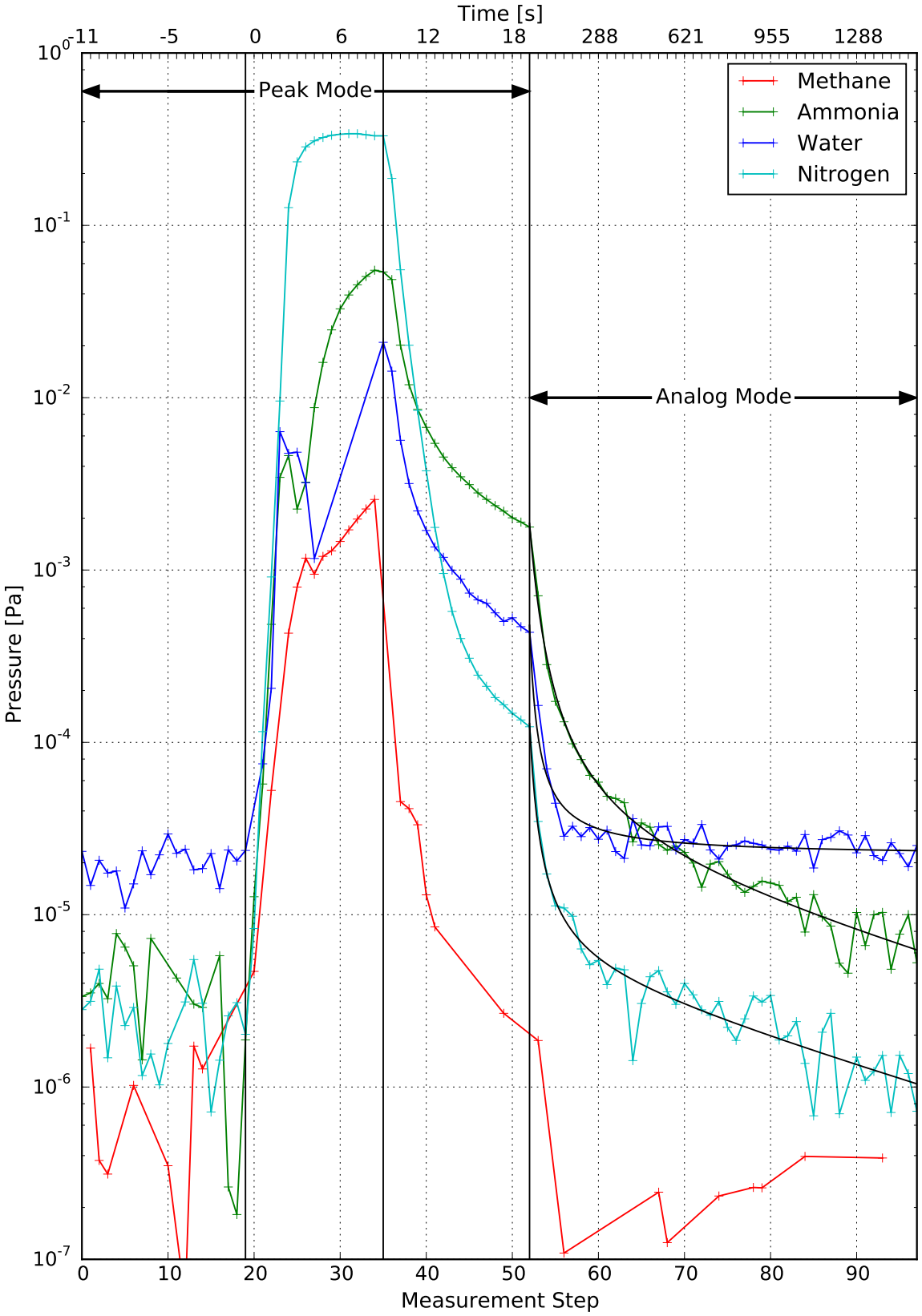

FIGURE 3.5: Fitted data multiplied with its calibration factor of discharge 34266 and device HPQI with exponential fits for the main impurities during analog measurement.

3.3 Calibration of Ammonia

As already mentioned in the last chapter the calibration procedure is not appropriate for sticking gases like ammonia. In figure 3.5 it is clearly visible that ammonia and water are the main impurity gases at the end of the peak mode for highly seeded discharges. Methane is only produced during the shot and due to it is not sticking on PFCs the amount of methane in the residual gas around 10 seconds after the discharge is negligible. Additionally water was already calibrated before. Using the minimization procedure on the last measurements of the peak mode for a highly seeded discharge it is possible to determine the cracking pattern of ammonia. Some unknown variables have to be fitted: the R value and intensity of both impurities and the cracking pattern/fragmentation vector of ammonia. If measurements of $m/z = 15$ to 20 are considered (14 is additionally polluted to nitrogen) it is possible to minimize

$$\begin{aligned} S = (&\gamma_{\text{Ammonia}} \cdot p.p._{\text{Ammonia}} \cdot \mathcal{A}_{\text{Ammonia}}(R_{\text{Ammonia}}) \cdot \vec{p}_{\text{Ammonia}} \\ &+ \gamma_{\text{Water}} \cdot p.p._{\text{Water}} \cdot \mathcal{A}_{\text{Water}}(R_{\text{Water}}) \cdot \vec{p}_{\text{Water}} - \vec{I})^2. \end{aligned} \tag{3.9}$$

The last 7 measurement points of the peak mode of discharge 34267 were used to calibrate the RGA for ammonia. Figure 3.6a shows that the fit, which is plotted by dashed lines, is matching very well the RGA intensities (solid lines). The residuals of all fits are small compared to the absolute intensities. Having a more detailed look at the fitted parameters like the partial pressure of the dominant impurities in figure 3.6b the assumption is valid that ammonia is the main impurity after the discharge while it is accompanied by some water. Around 20 seconds after the beginning of the discharge around 60% of the impurity gases which contribute to $m/z = 15$ - 20 is ammonia. The resulting fragmentation vector for ammonia in figure 3.6d is nearly constant for all fitting points and results in

$$\vec{p}(\text{Ammonia, HPQI}) = (1, 0.60, 0.034, 0)^{\text{T}}. \tag{3.10}$$

The last entry of the fragmentation vector of ammonia was not determined because $m/z = 14$ is dominated by nitrogen. The contribution of $m/z = 14$ should be about one order less than the preceding fragmentation level which is at 0.034.
The results of the calibration for other devices can be seen in appendix C.

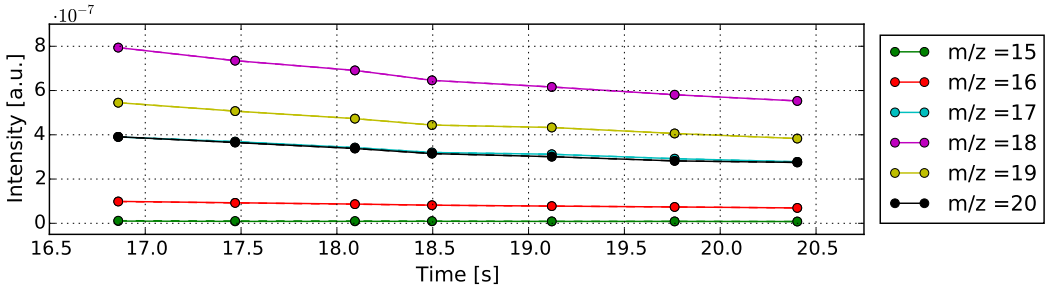

(a) Raw Data (solid lines) with its fitted intensities (dashed lines (mostly overlapped by the solid lines))

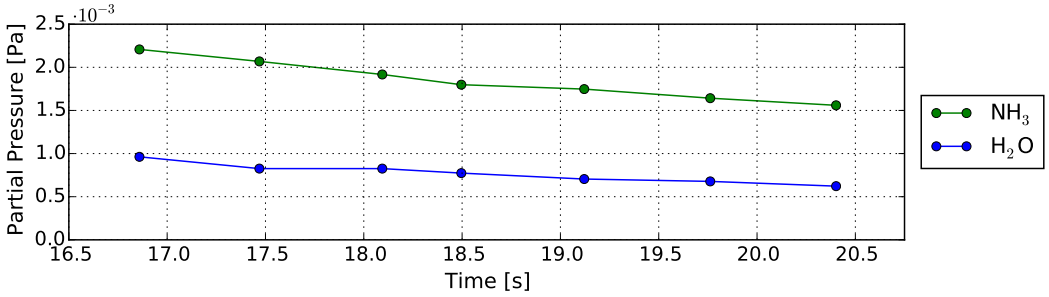

(b) Fitted partial pressures of considered impurity gases water and ammonia

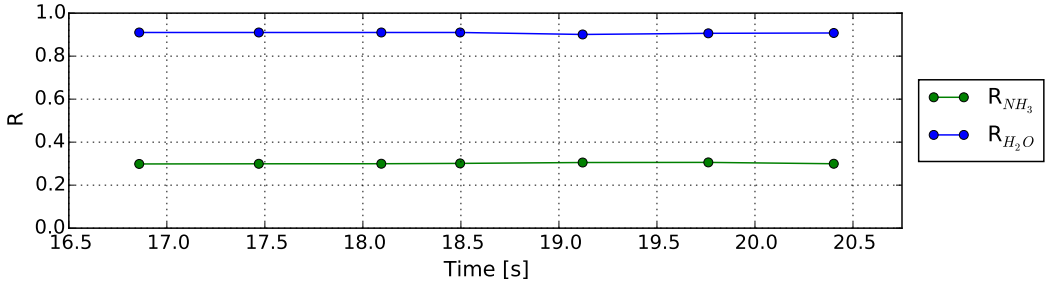

(c) Fitted R values of considered impurity gases water and ammonia

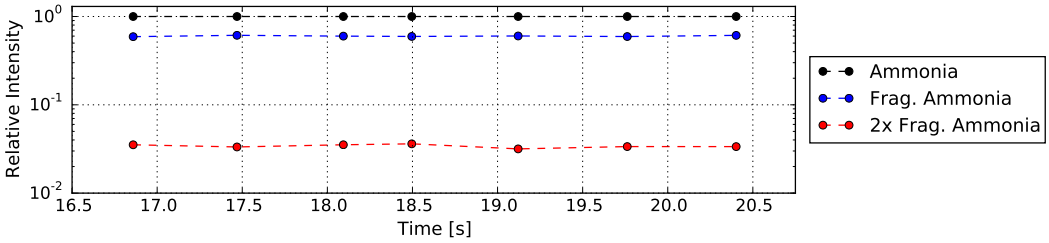

(d) Fitted cracking pattern of ammonia

FIGURE 3.6: HPQI: Fitting cracking pattern of ammonia for the last 7 measurement points in peak mode of discharge 34267 (2017-05-23)

A comparison of the fitting results for the identified partial pressure and the residuals for the default and calibrated cracking pattern of ammonia should be done to identify if the calibration returns better results. The default cracking

pattern (calibration done in October 2016) for ammonia was

$$\vec{p}(\text{Ammonia, HPQI}) = (1, 0.80, 0.065, 0)^{\mathrm{T}} \tag{3.11}$$

and differs from the calibrated cracking pattern 3.10. Figure 3.7a shows the fitted partial pressures during peak mode for discharge 34267. While both fits are the same during the discharge a clear difference of about 20% can be seen in the after discharge phase. The residuals of both fits in this phase are different up to a factor of 10 (see figure 3.7b). If the new cracking pattern is used the residual is much lower, which indicates that the fit is better. Therefore it can be assumed that if the old cracking pattern is used ammonia is substituted into other impurities and the resulting partial pressures of ammonia are underestimated during the outgassing phase.

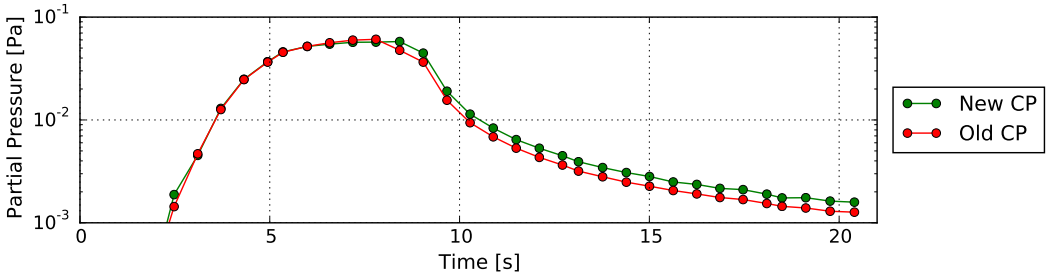

(a) Fitted partial pressures of ammonia for the default and calibrated cracking pattern

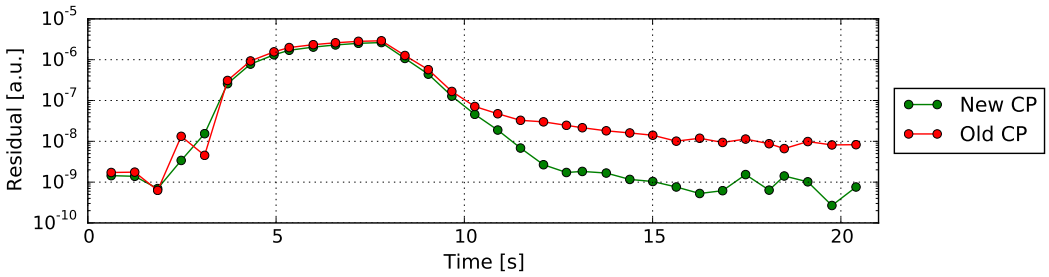

(b) Residuals of the fittings for the default and calibrated cracking pattern

FIGURE 3.7: HPQI: Comparison of default and calibrated cracking pattern of ammonia for the last 7 measurement points in peak mode of discharge 34267 (2017-05-23)

Chapter 4

Nitrogen Enrichment in N_2 Puffed Discharges

To investigate the amount of nitrogen in the plasma measuring the nitrogen content in the residual gas could be a first approach. But the residual gas doesn't have to reflect the plasma mixture necessarily. Commonly nitrogen is puffed into the divertor from the X valves (see figure 2.1). A part of the seeded nitrogen doesn't interact with the plasma because of a low penetration probability and is pumped out directly. This part would be recognized in the residual gas but never interacted with the plasma itself.
A second important point to consider is the seeding location. The DuX valves are used to seed nitrogen. Dependent on the amount of seeding some of the valves are not used. This could lead to local effects of the seeding which could be seen not only in the mixture of the residual gas but also in the pressure measurements by the baratrons at different locations.
First the evaluated discharges are introduced with a comparison between a non-seeded and seeded discharge. Then local puffing effects of nitrogen are discussed in more detail and at the end a discussion about the nitrogen content in the plasma and the nitrogen to ammonia conversion in ASDEX Upgrade follows.

4.1 Global Parameters of Evaluated Discharges

For the assessment of the nitrogen enrichment in N_2 seeded discharges three sets of discharges with in total 16 shots were evaluated. They were performed on three different days: 2017-05-05, 2017-05-23 and 2017-06-29. All discharges reached the high confinement regime. The global parameters are shown in tables 4.1, 4.2 and 4.3. n_e is the line averaged electron density, I_p is the plasma current and P_{tot} is the total heating power which was provided by neutral beam injection (NBI), electron cyclotron resonance heating (ECRH) and ion cyclotron resonance heating (ICRH). Additionally the total amount of puffed nitrogen during the discharge is given.

4.1.1 Discharge Set 34156 - 34163

Shotnumber	34156	34157	34158	34159	34160	34162	34163
Plasma density n_e $[\cdot 10^{19} m^{-3}]$	7.79	7.27	6.42	6.49	6.01	2.86	-
Plasma current I_p [MA]	0.60	0.60	0.60	0.60	0.60	0.80	1.002
Total heating power P_{tot}[MW]	9.193	10.270	10.450	9.213	9.263	2.491	4.948
Total puffed N_2 $[\cdot 10^{21}$ #$N_2]$	4.89	1.86	1.52	1.59	3.46	-	-
N_2 puffing valves	Du05X, Du13X						

TABLE 4.1: Global Parameters for discharges 341xx

4.1.2 Discharge Set 34264 - 34270

Shotnumber	34264	34265	34266	34267	34269	34270
Plasma density n_e $[\cdot 10^{19} m^{-3}]$	5.53	5.58	6.42	6.49	6.01	7.74
Plasma current I_p [MA]	0.60	0.60	0.60	0.60	0.60	0.80
Total heating power P_{tot}[MW]	9.193	10.270	10.450	9.213	9.263	4.892
Total puffed N_2 $[\cdot 10^{21}$ #$N_2]$	3.74	5.01	11.2	9.44	-	-
N_2 puffing valves	Du01X, Du09X, Du13X					

TABLE 4.2: Global Parameters for discharges 342xx

4.1.3 Discharge Set 34532 - 34535

Shotnumber	34532	34533	34535
Plasma density n_e $[\cdot 10^{19} m^{-3}]$	7.47	8.33	8.96
Plasma current I_p [MA]	0.80	1.002	1.020
Total heating power P_{tot}[MW]	5084	5.917	5.083
Total puffed N_2 $[\cdot 10^{21}$ #$N_2]$	3.37	-	-
N_2 puffing valves	Du01X, Du09X		

TABLE 4.3: Global Parameters for discharges 3453x

4.2 Comparison of Non-Seeded and Seeded Discharges

In the three sets of discharges first seeded shots were performed. During the seeded discharges a part of the nitrogen is retained and builds up a nitrogen

inventory. Afterwards similar non-seeded discharges were performed which allowed a more detailed look on the ammonia production because they only deal with retained nitrogen.
For a first comparison a non-seeded (without pre-load of nitrogen) and a seeded discharge are compared: discharge 34195 and 34267.

4.2.1 Non-seeded Discharge 34195

Figure 4.1 illustrates the main plasma parameters for discharge 34195. The sub-figures 4.1 a), b) and c) show the plasma current I_p , the toroidal magnetic field B_T and the line averaged plasma density n_e in the midplane respectively. In the next plot the heating power is illustrated, which consists of electron cyclotron resonance heating (ECRH, red line) and neutral beam injection (NBI, blue line). The total power stays roughly constant at about 6 MW throughout the discharge except some blips which are needed for diagnostic measurements like charge exchange recombination spectroscopy (CXRS). In sub-figure e) the pressure at the inner divertor (blue line) and the outer divertor (red line) can be seen. In the last one the applied flux of deuterium (blue line) is visible. In

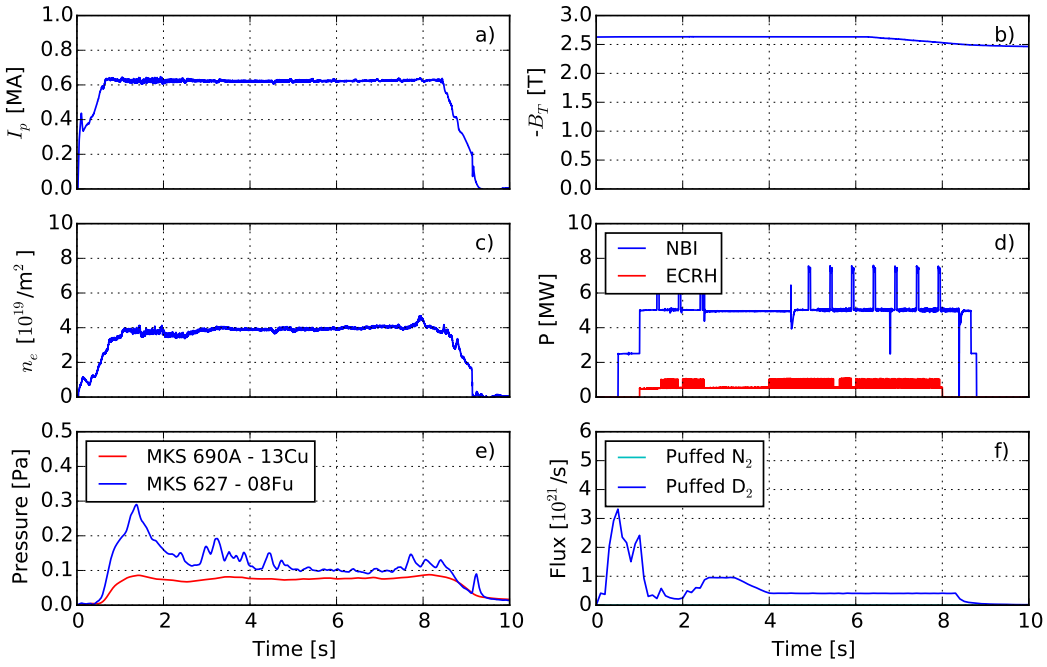

FIGURE 4.1: a) Plasma current I_p, b) toroidal magnetic field B_T, c) line averaged electron density n_e, d) heating power of ECRH (red line) and NBI (blue line), e) pressure at inner divertor (blue line) and outer divertor (red line) and f) injected deuterium (blue line) flux during non-seeded H-mode discharge 34195 (nitrogen flux during this discharge is 0)

figure 4.2 the measured intensities for $m/z = 14 - 20$ and 28 before, during and after the non-seeded discharge 34195 are shown. The highest intensities

are $m/z = 18$ and 20 which corresponds to highly deuterated impurities. The third highest intensity is $m/z = 28$ which corresponds to nitrogen. It is followed by other impurity m/z ratios like 16, 17 and 19. Very small intensities are measured at $m/z = 14$ which is still dominated by fragmented nitrogen which can be seen on the same shape like $m/z = 28$. $m/z = 15$ is during the whole measurement phase up to 3 orders of magnitude smaller than other measured intensities. After the discharge all intensities . After several hundreds of seconds $m/z = 18$ is the largest measured intensity which can be connected with background water.
The results of the minimization procedure can be seen in figure 4.3. During the discharge phase methane, nitrogen and water have the same order of magnitude at around $5 \cdot 10^{-4}$ Pa, while ammonia is not present at all. Nitrogen and methane are dropping after a few 100 seconds after the discharge to noise level, water is only decreasing by roughly one order of magnitude back to a background level of $2 \cdot 10^{-5}$ Pa.

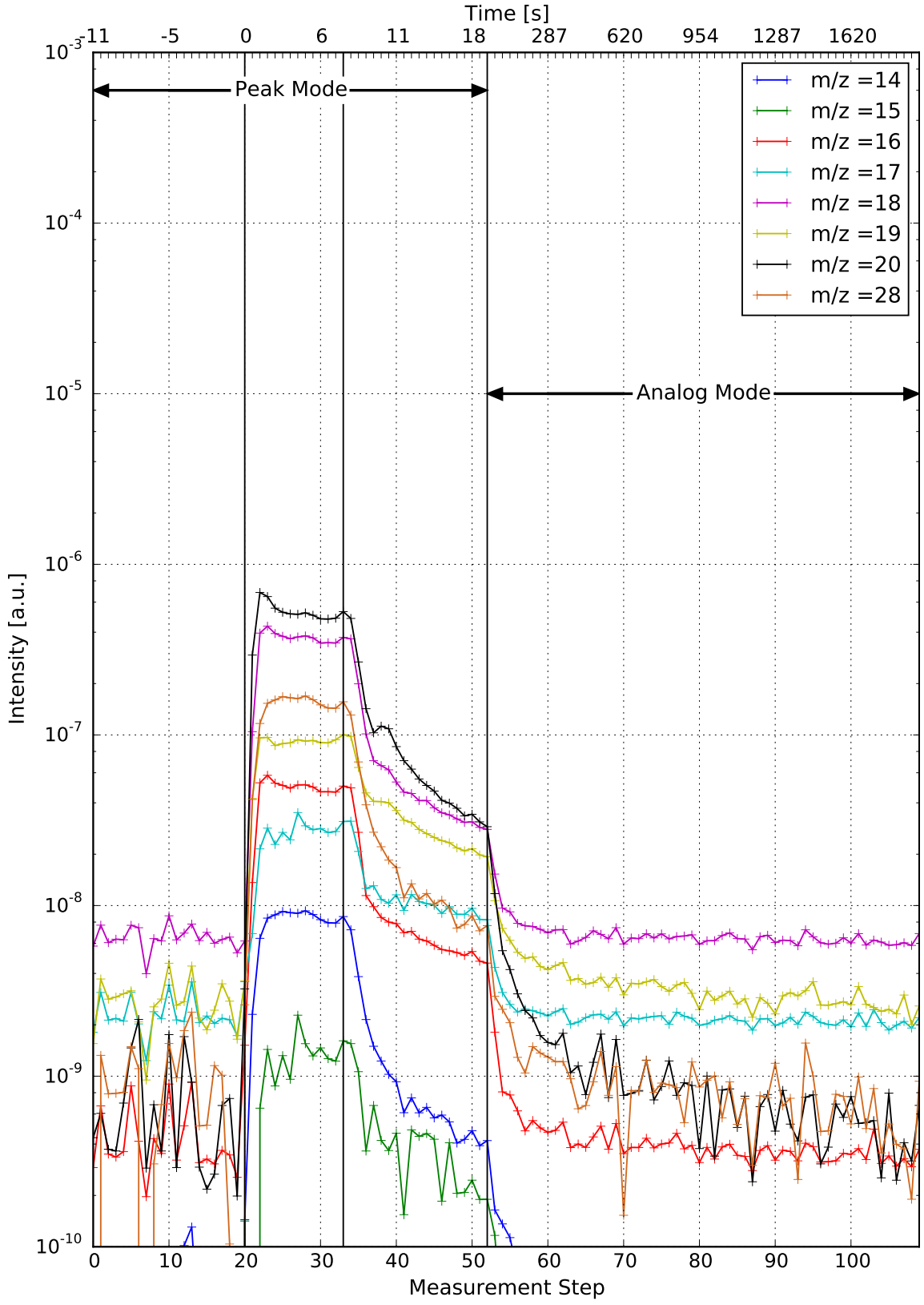

FIGURE 4.2: Corrected raw data of discharge 34195 and device HPQI

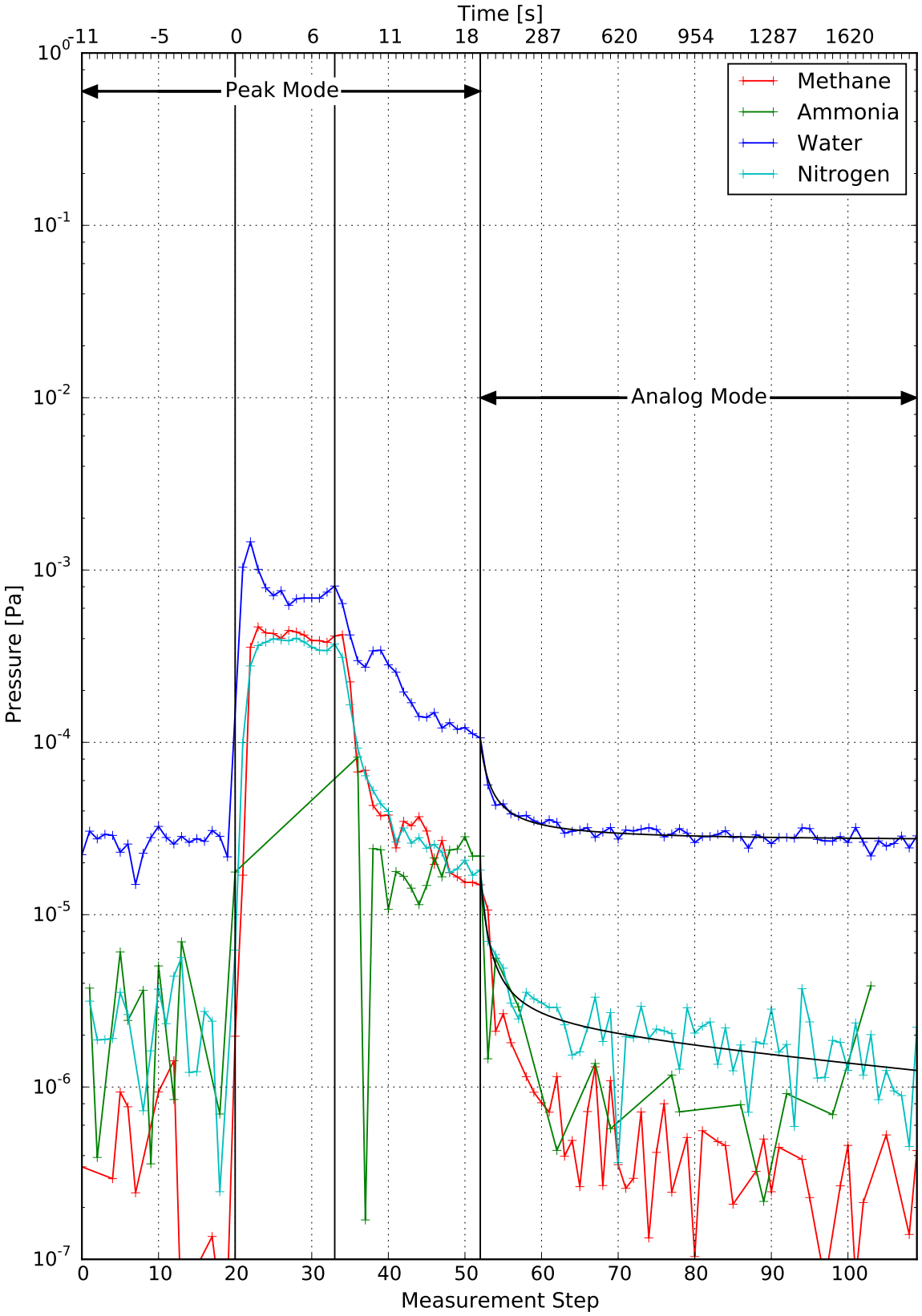

FIGURE 4.3: Fitted partial pressures of non-seeded discharge 34195 and device HPQI with exponential fits for main impurities for extrapolation to out-gassing

4.2.2 Seeded Discharge 34267

Figure 4.4 illustrates the main plasma parameters for discharge 34267. While the plasma current I_p and the toroidal magnetic field B_T are roughly the same compared to the non-seeded discharge, the line averaged plasma density n_e in the core region, the heating power and the puffing rate of deuterium are enhanced. This leads also to much higher pressures in the divertor region. In

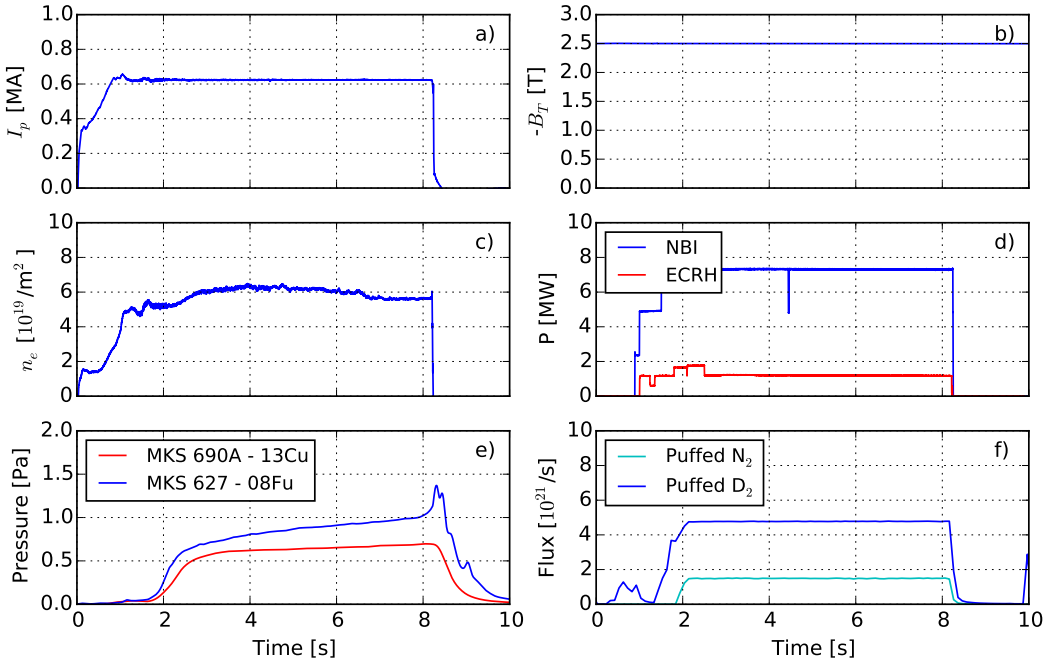

FIGURE 4.4: a) Plasma curren I_p, b) toroidal magnetic field B_T, c) line averaged electron density n_e, d) heating power of ECRH (red line) and NBI (blue line), e) pressure at inner divertor (blue line) and outer divertor (red line) and f) injected deuterium (blue line) and nitrogen (cyan line) flux during seeded H-mode discharge 34267

figure 4.5 the measured intensities for m/z = 14 - 20 and 28 before, during and after the discharge 34267 are shown. Three main groups of intensities can be seen during the discharge. m/z = 28 is much higher compared to all other intensities because of the nitrogen puffing during the discharge, already shown in discharge 34266. The second group is about one order of magnitude lower and consists of m/z = 14 which is dominated by the puffed nitrogen which is fragmented in the ion source of the RGA and m/z = 17 - 20 which represents the impurity mixture of methane, water and ammonia. The smallest intensities are measured for m/z = 15 and 16 which are high fragmented or protonated impurities. After the discharge all intensities decline by several orders, especially m/z = 28 is dropping much faster than the others. After several hundreds of seconds m/z = 18 is the largest measured intensity which can be connected with background water, like for discharge 34195.

The minimization procedure calculated the partial pressures of the impurity gases which can be seen in figure 4.6. As already indicated before nitrogen is the most abundant impurity beside ammonia. After the discharge nitrogen is dropping much faster than water or ammonia, while methane is dropping already after a few seconds back to the noise level. Important to mention is that ammonia is throughout the whole after-discharge phase around one order of magnitude larger than nitrogen because of nitrogen seeding during the shot. It is additionally enhanced by retained nitrogen from previous N_2 seeded discharges. At the end of the discharge the background level of water can be seen which is at around $2 \cdot 10^{-5}$ Pa.
While for a non-seeded discharge methane, nitrogen and water are at around $5 \cdot 10^{-4}$ Pa and ammonia is not even present during the discharge, this seeded discharge behaves totally different. By far the most abundant gas is nitrogen (roughly 1000 times higher) followed by ammonia which is created by the puffed N_2.

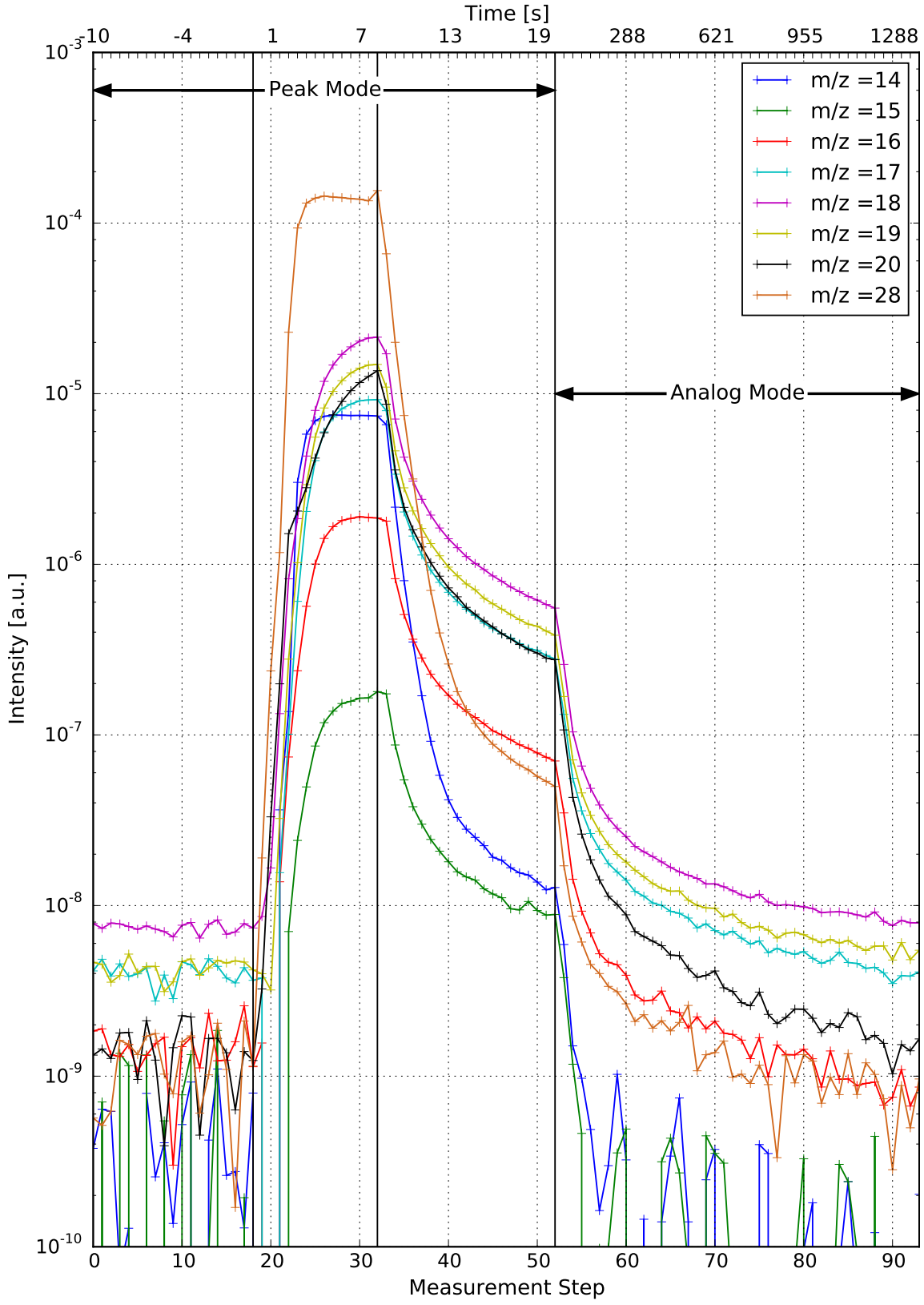

FIGURE 4.5: Corrected raw data of discharge 34267 and device HPQI

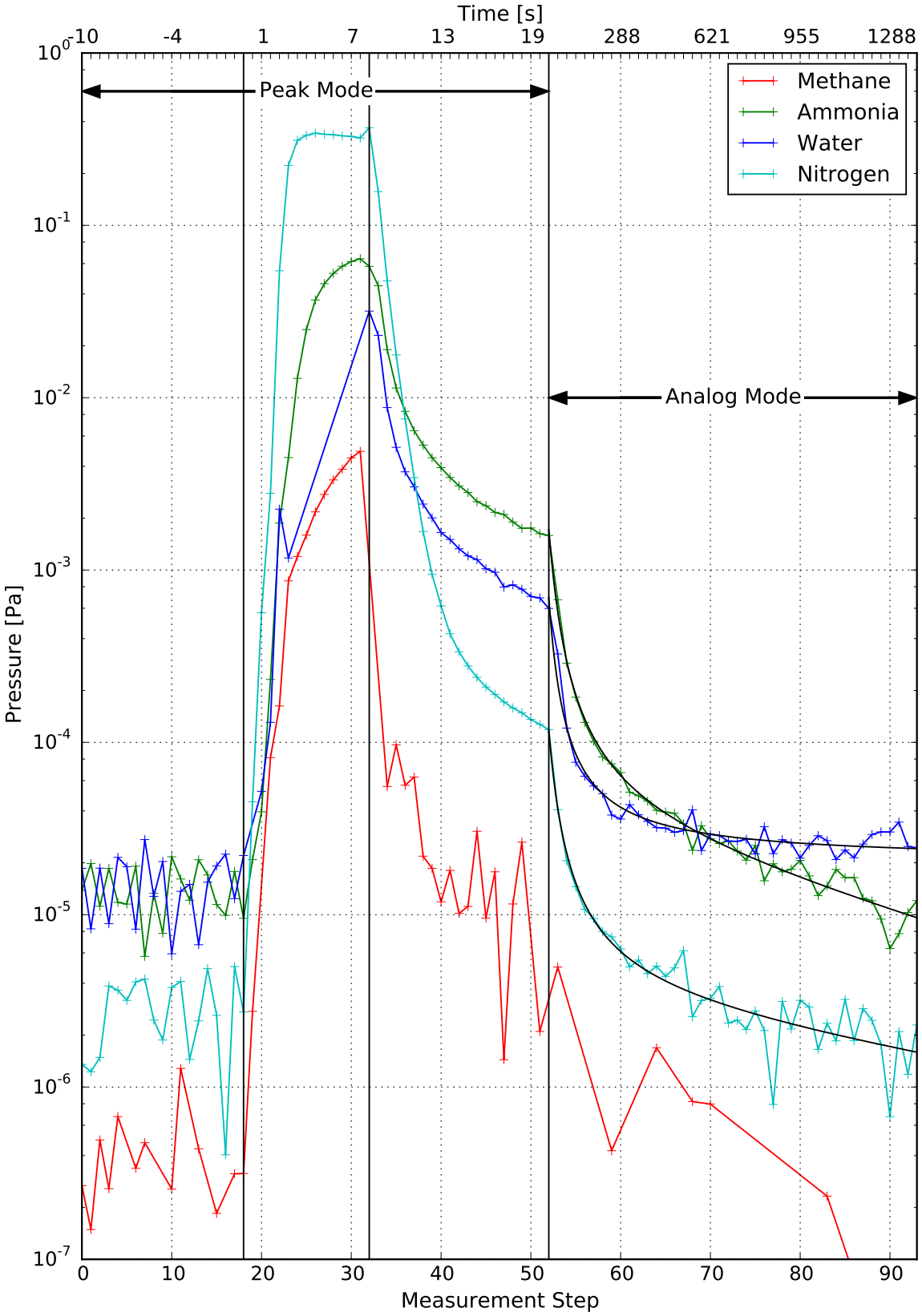

FIGURE 4.6: Fitted partial pressures of highly seeded discharge 34267 and device HPQI with exponential fits for main impurities for extrapolation to out-gassing

4.3 Local Effects of Nitrogen Seeding

For a closer look on such a local effect of nitrogen seeding two similar discharges are compared. Especially the nitrogen signal ($m/z = 28$) of the RGAs, the related pressure measurements are compared in more detail.

4.3.1 Comparison of discharge 34266 and 34532

To get a first impression on such a local seeding effect two similar discharges, 34266 and 34532, with different seeding characters are compared. For shot 34266 the valves Du01X, Du09X and Du13X where used for nitrogen seeding while the valves Du01B, Du09B, Du13B were used for deuterium refueling. In contrast to that only Du01X and Du09X (for nitrogen) and Du01B and Du09B (for deuterium) were used for discharge 34532 (see table 4.4). Figure 4.7 shows

	Du01		Du05		Du09		Du13	
	B	X	B	X	B	X	B	X
34266	D_2	N_2			D_2	N_2	D_2	N_2
34532	D_2	N_2			D_2	N_2		

TABLE 4.4: Usage of valves for D_2 and N_2 seeding during discharges 34266 and 34532

the local positions of the valves which were used during these two discharges and the mass spectrometers in the torus. As the RGA HPQO is in the outer divertor in sector 13, where once fueling/seeding is present and once not, this difference could lead to a local effect which should not only observable in the RGA data but also in the total pressure data.
The upper two graphs in figure 4.8 show the measured total pressure near the RGAs by MKS 627 in the inner divertor with the signal name 'B02_Fu08' and the MKS 690A in the outer divertor with the signal name 'B01_Cu13'. The two graphs in the middle show the measured partial pressures of nitrogen which were measured by the RGA HPQI in sector 8 and HPQO in sector 13. The lower graphs show the puffing/refueling rates of nitrogen and deuterium in the specific sector regions.
During discharge 34266 (blue lines) the puffing rates for nitrogen and deuterium are in both sectors the same, while in 34532 (red lines) no gas was puffed in sector 13 at all. To have the same overall refueling and puffing rate the rate in sector 9 has to be roughly 3/2 higher than for discharge 34266.
The high puffing rates in both discharges in sector 8 lead to a significant amount of nitrogen in the residual gas nearby the RGA HPQI. The measured partial pressure of N_2 is illustrated as filled circles in the middle plots. While the peak intensity of both shots in sector 8 is roughly the same, a clear difference can be seen in sector 13 where neither D_2 nor N_2 was puffed during discharge 34532. The maximum partial pressure of nitrogen for that shot is

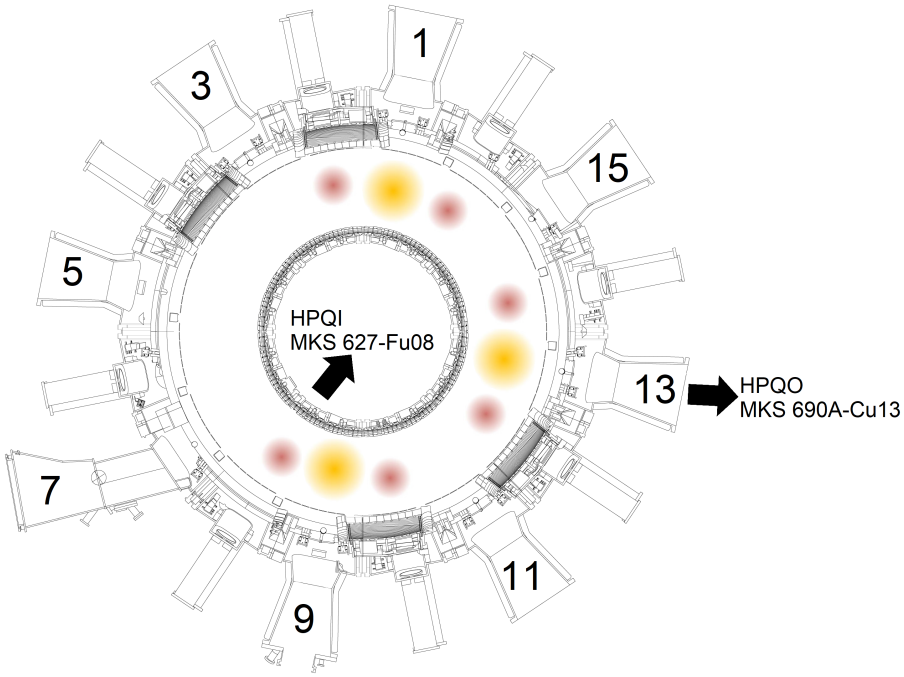

FIGURE 4.7: Local positions of valves in the torus and used mass spectrometers HPQI and HPQO

only a sixth of that of discharge 34266.
This local behavior is also observed in the total pressure measurements at the same locations as the RGAs. While the total pressures of both shots in sector 8 are roughly the same, the pressures in sector 13 are different by a factor of two, around 0.35 Pa for 34532 while it is 0.65 Pa for 34266. This pressure difference can be explained by the usage of the puffing valves in sector 13: While for discharge 34266 the partial pressure of nitrogen is around 0.1 Pa and it is assumed that the pressure is linear to the puffing rate of deuterium which is three times larger than that for nitrogen a rough pressure difference of 0.4 Pa should be observable. Indeed the difference in total pressure is around 0.3 Pa.

Worth mentioning is the pressure decrease in the inner divertor for discharge 34266 at around 3 s. The high field side high density front is reduced by nitrogen seeding which leads to a lower pressure in the inner divertor [24]. By having a closer look to the pressure measurement of shot 34532 in figure 4.8 this effect can also be seen at around 6 s. As the nitrogen is accumulating in the inner divertor the HFSHD front is weakened and the pressure drops of about 10%.

A clear local seeding effect can be seen by the comparison of the two shots. For a more general look at this effect the whole campaign of 2017 was examined in more detail.

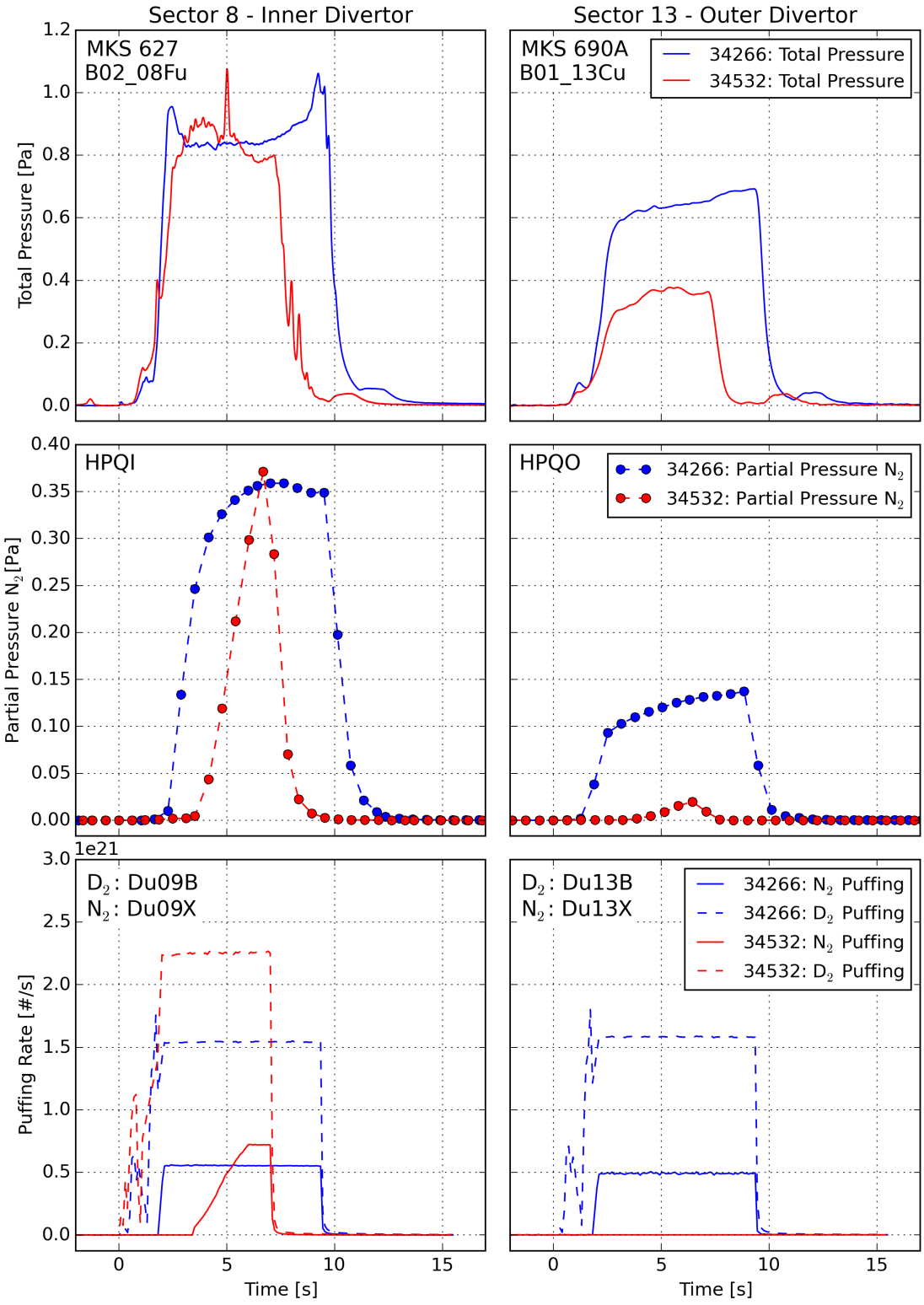

FIGURE 4.8: Comparison of total pressure, N_2 partial pressure and D_2, N_2 seeding at sector 8/9 and 13 during discharge 34266 and 34532.

4.3.2 Local Seeding Effect for Campaign 2017

The local effect which was described earlier could also be an effect for only these two discharges which were compared. Therefore more nitrogen seeded discharges have to be compared to see if this is a general behavior. As database the ASDEX Upgrade campaign 2017 was used for studying this effect.
The integrated nitrogen intensities of the RGAs HPQI and HPQO were compared with the total seeded amount of nitrogen during each shot. For a better discharge comparison shots with following properties were excluded:

- discharges with $I_p \leq 550$ kA,
- usage of killergas and
- disrupted discharges.

If the plasma current of a discharge is smaller than 550 kA it was not successful and therefore not useful for the comparison. A killergas, like Neon, is used to prevent the plasma facing components of damages by heavy disruptions. Large amounts of the killergas are injected during disruptions to cool the plasma. The killergas in the residual gas leads to a misinterpretation of the measurements because of the domination at specific m/z ratios of the impurity. In figure 4.9 the results for HPQI are shown. One circle represents

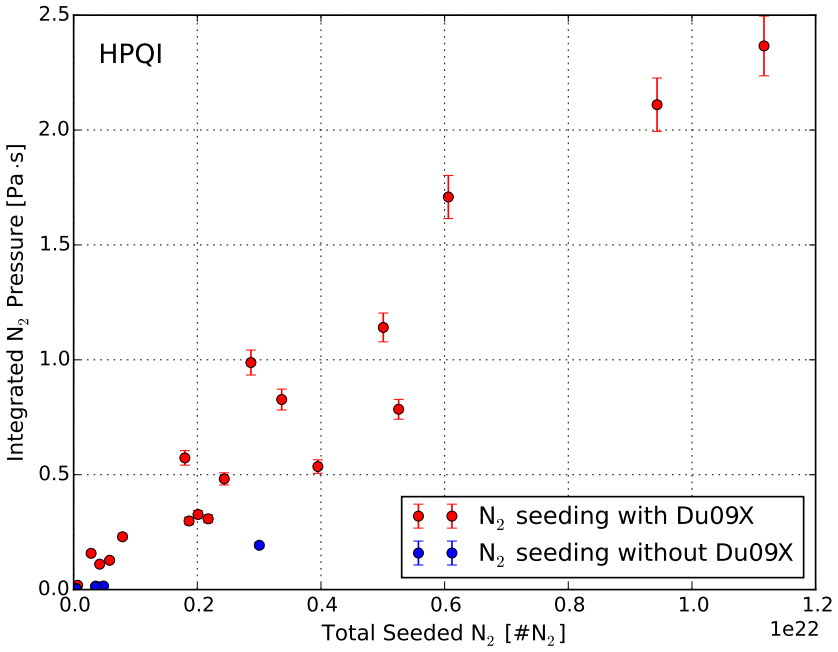

FIGURE 4.9: Comparison of integrated partial pressure intensities of nitrogen measured by HPQI for different seeding procedures: red points are seeded with valve Du09X, while blue points are representing discharges where this valve was not used.

one seeded discharge. The red points are shots where valve Du09X was used

for seeding and the blue ones are shots where the valve next to the RGA was not used. The measured intensities rise more quickly with the total amount of seeded nitrogen if it is also seeded in the region where measurement takes place. On the other hand, discharges which are not seeded with valve Du09X for HPQI, the integrated amount of nitrogen is clearly not rising so quickly. This indicates that most of the nitrogen which is puffed next to the RGA is pumped out directly in that region and does not spread symmetrically around the torus.
But still some integrated intensities are low compared to others for discharges where valve Du09X was used. This behavior comes from the number of used valves: if the same amount of nitrogen is puffed with four valves at the same time a smaller amount will be puffed by the local valve Du09X compared to a discharge where only two valves are used for seeding. This leads to a lower integrated intensity.

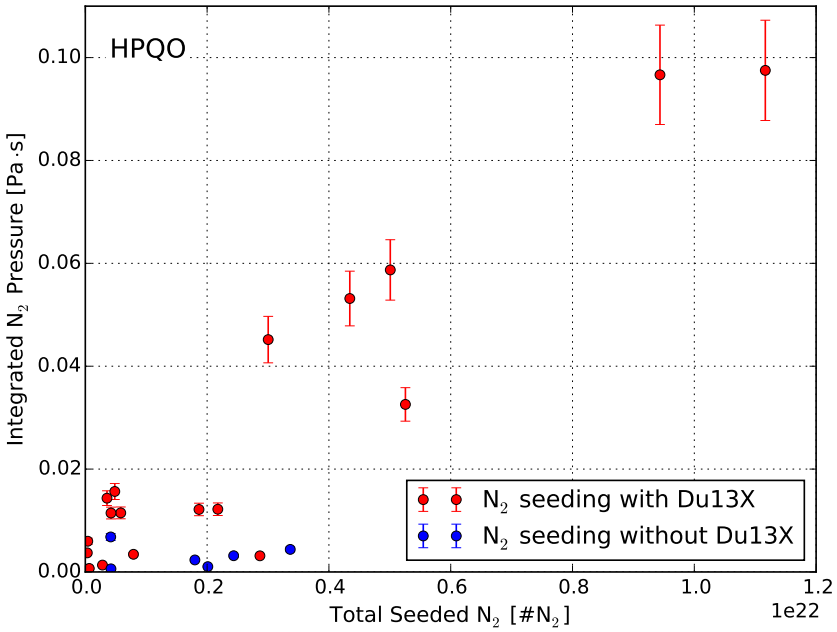

FIGURE 4.10: Comparison of integrated partial pressure intensities of nitrogen measured by HPQO for different seeding procedures: red points are seeded with valve Du13X, while blue points are representing discharges where this valve was not used.

This local effect can also be seen in the outer divertor for HPQO in sector 13. In figure 4.10 the same dependencies can be drawn. When nitrogen is seeded directly next to the RGA the measured intensity is much larger than for discharges where the Du13X valve is not used.

While neutral nitrogen is directly pumped ammonia is produced with help of the plasma, so a more homogeneous behavior is expected. To test this, the fitting procedure described before was executed for all seeded discharges of the

same database already seen in figure 4.9 for HPQI, and the resulting partial pressures of ammonia were integrated. Figure 4.11 does not show a difference between the offsets of red and blue discharges, but the integrated amount of ammonia in discharges in which nitrogen was not puffed with valve Du09X show comparable intensities. Also for HPQO (see figure 4.12) no clear offset

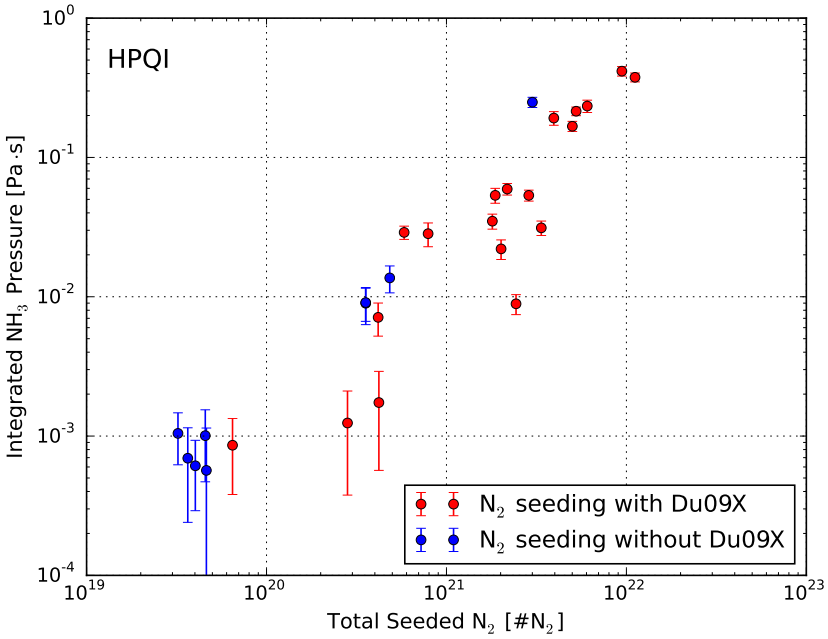

FIGURE 4.11: Comparison of integrated partial pressure intensities of ammonia measured by HPQI for different seeding procedures: red points are seeded with valve Du09X, while blue points are representing discharges where this valve was not used.

difference in the data can be seen.
Such a local effect which was clearly observed for nitrogen is not observable for ammonia in the inner or outer divertor.

4.3.3 Conclusion

The subsections before pointed out a strong influence of the local seeding effect on mass spectrometer measurements of nitrogen. The measured intensity did not only depend on the amount of seeded impurity atoms or the seeding flux, but also on the used impurity seeding valves. This makes the measurement of nitrogen in the residual gas as an indicator of the amount of nitrogen in the divertor plasma not independent on local parameters for all seeded discharges. If most of the puffed nitrogen is not ionized due to a low penetration probability the toroidal spread is not large and most of the N_2 is pumped out of the vessel locally at the puffing location. Therefore a large amount of nitrogen can be detected by the RGAs locally. But if nitrogen is becoming ionized it has to follow the magnetic field and therefore the toroidal transport is much better

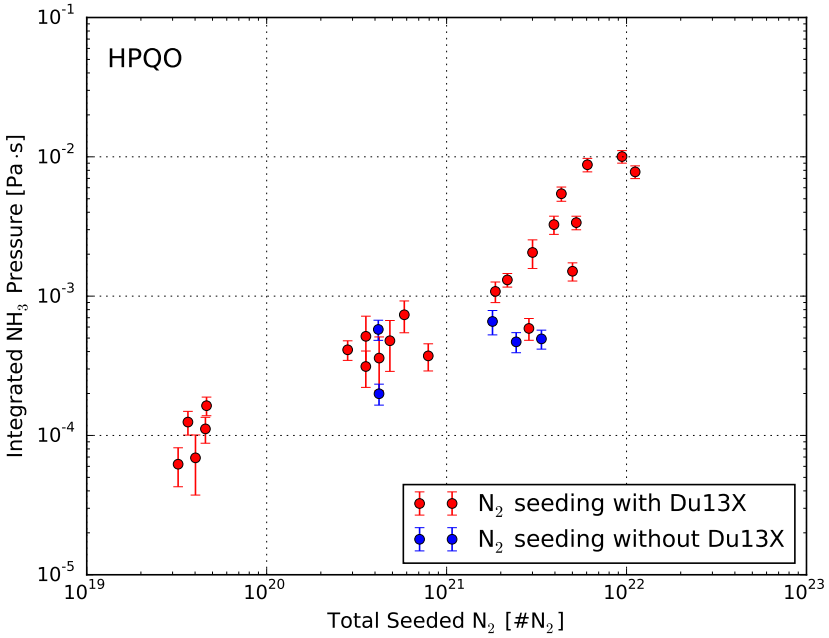

FIGURE 4.12: Comparison of integrated partial pressure intensities of ammonia measured by HPQO for different seeding procedures: red points are seeded with valve Du13X, while blue points are representing discharges where this valve was not used.

i.e. it is distributed equally around the torus. Therefore another option to measure the nitrogen content in the divertor plasma is the measurement of ammonia which is produced by recombination with deuterium. It could be seen that such a local effect is not visible for ammonia.

4.4 Comparison of Impurity Signal of CXRS with RGA Data

Out of charge exchange recombination spectroscopy (CXRS) data the nitrogen impurity in the main plasma can be calculated. By comparison of the integrated nitrogen amount in the plasma with the integrated nitogen and ammonia signals of the RGAs it can be shown which of them can be a good indicator for the nitrogen in the divertor plasma.
In total out of the 16 evaluated discharges for this thesis it was possible to gain impurity density data by the CXRS of 13 discharges. Figure 4.13 shows the

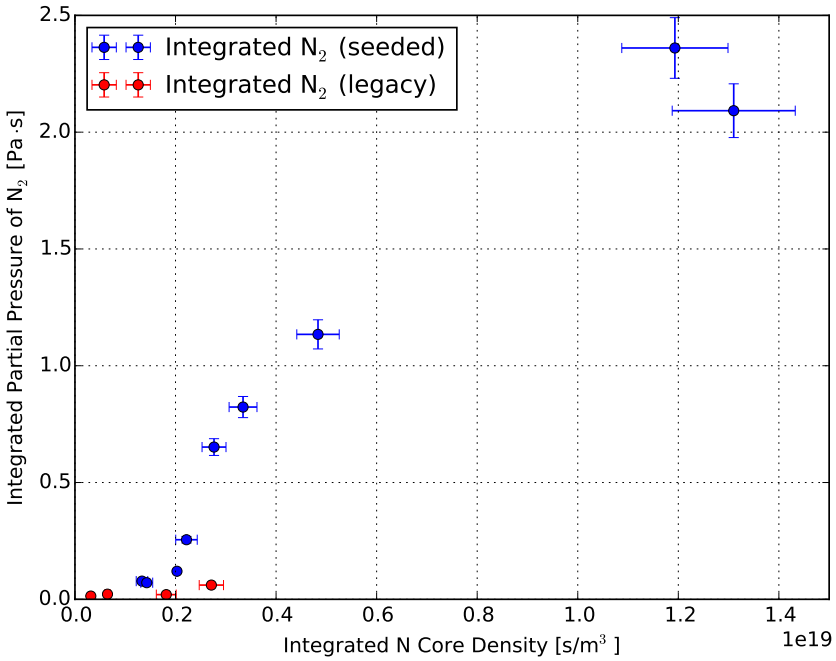

FIGURE 4.13: Comparison of integrated CXRS nitrogen core density and the integrated partial pressure of nitrogen (HPQI)

results of the comparison between the integrated nitrogen amount in the core plasma with the integrated partial pressure of nitrogen for HPQI for seeded and legacy discharges (non-seeded shots after seeded discharges). Around 8 discharges have a small value for the integrated partial pressure of nitrogen while the impurity data is varying by a factor of 3 or more. The other 5 discharges have both large intensities for the integrated nitrogen density and the integrated partial pressures. But two different branches are visible, one for the seeded and one for non-seeded discharges which is a clear evidence that the neutral gas does not always represent the plasma N content. Therefore the directly measured nitrogen as indicator is not good.
Because the nitrogen measurement is dependent on the seeding behavior the integrated ammonia signal was compared with the integrated nitrogen density in the core plasma. In figure 4.14 the dependency between the integrated

CXRS nitrogen impurity data and the integrated ammonia can be seen. The

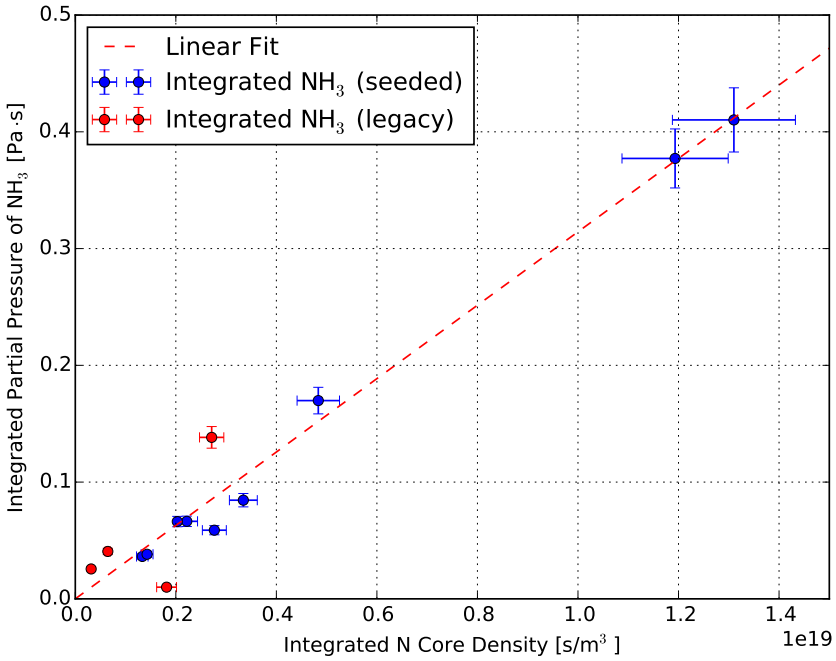

FIGURE 4.14: Comparison of integrated CXRS nitrogen core density and the integrated partial pressure of ammonia (HPQI)

data suggest a linear and direct behavior between the amount of created ammonia and the integrated nitrogen content in the core plasma. No difference for seeded and non-seeded discharges is visible. This direct behavior suggests that the integrated ammonia signal is also an indication of the amount of nitrogen in the divertor plasma.

4.5 Assessment of Nitrogen Enrichment by Correlation Factor

The comparison of the CXRS data and the ammonia signals of the RGA leads to the usage of that signal for an estimation of the nitrogen signal in the divertor plasma.
The result of the fitting routine leads to partial pressures of the considered residual gases. In figure 4.6 this was already done for discharge 34267. The high amount of ammonia in the residual gas especially after the discharge from around $t = 10$ s till the end of the analog mode compared to nitrogen should be noted. Because ammonia is sticking on plasma facing components the created ammonia needs more time to reach the pumps and the mass spectrometer. Therefore a time-dependent evaluation during a shot is strongly affected.
To determine the nitrogen content in divertor plasma the so called correlation

factor was calculated which is defined by

$$\text{Correlation Factor} = \frac{\int_0^{\text{BG}} I_{\text{Ammonia}}(t)dt}{\int_0^{\text{BG}} I_{\text{Nitrogen}}(t)dt}. \tag{4.1}$$

The integral is performed from the start of the shot till the partial pressure signal has reached the background level (BG). The background is calculated by the mean value of the fitted partial pressures before the shot (t < 0 s).
During and after the shot (but still during the peak mode) the fitted partial pressures were integrated using the trapezoidal rule. Due to the fitted intensities are not smooth anymore in the analog data an exponential function was fitted and integrated till it reaches the background level.
The main idea is that if the retained nitrogen is detected by the residual gas analyzers during legacy shots it had to interact with the plasma before. The nitrogen therefore has a specific probability to form ammonia. This fraction should be constant during all legacy discharges for a specific device. Geometrical or pumping issues can lead to different legacy correlation factors for different devices.
This constant factor of the legacy discharges can be applied then onto the measured ammonia intensities of seeded discharges to calculate the amount of nitrogen which interacted with the plasma.

4.5.1 Legacy Discharge 34269

As an example, legacy discharge 34269 is described which is the subsequent discharge after 34267 (because discharge 34268 was aborted after one second due to a disruption) is shown. Figure 4.15 describes the evolution of the global parameters. While the plasma current, the toroidal magnetic field, the line averaged electron density and the total heating of ECRH and NBI are comparable to the seeded discharge 34267 (see figure 4.4), the deuterium flux is enhanced by a factor of 2. Also the divertor pressure is completely different. While the pressure in the outer divertor is enhanced a bit, the inner divertor pressure is much higher compared to discharge 34267. Because of no nitrogen seeding the HFSHD front is not weakened which leads to the larger pressure in the inner divertor for the legacy shot.
For a direct comparison between a seeded and legacy discharge the fitted partial pressures of nitrogen and ammonia of seeded discharge 34267 and legacy discharge 34269 can be seen in figure 4.16. While the nitrogen signal for the seeded discharge is at around $4 \cdot 10^{-1}$Pa the pressure during the legacy discharge is smaller by a factor of 30 to 40. In comparison the ammonia pressure is only dropping by a factor of 3 to 4 compared to the seeded discharge.
While N_2 is dominating the residual gas compared to ammonia during 34267, the ammonia pressure is similar or even a higher than nitrogen for 34269.
After the discharge nitrogen and ammonia are behaving similar in both discharges. Nitrogen is dropping much faster, while ammonia sticks on PFCs and needs therefore more time to be pumped out of the vessel.

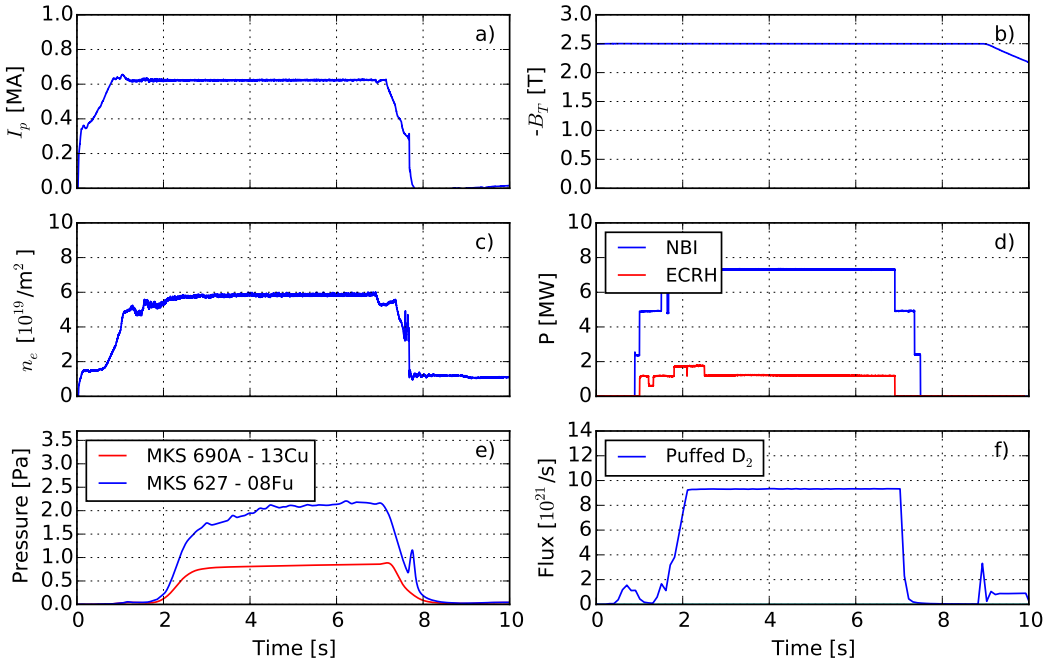

FIGURE 4.15: a) Plasma curren I_p, b) toroidal magnetic field B_T, c) line averaged electron density n_e, d) heating power of ECRH (red line) and NBI (blue line), e) pressure at inner divertor (blue line) and outer divertor (red line) and f) injected deuterium (blue line) flux during non-seeded H-mode discharge 34269

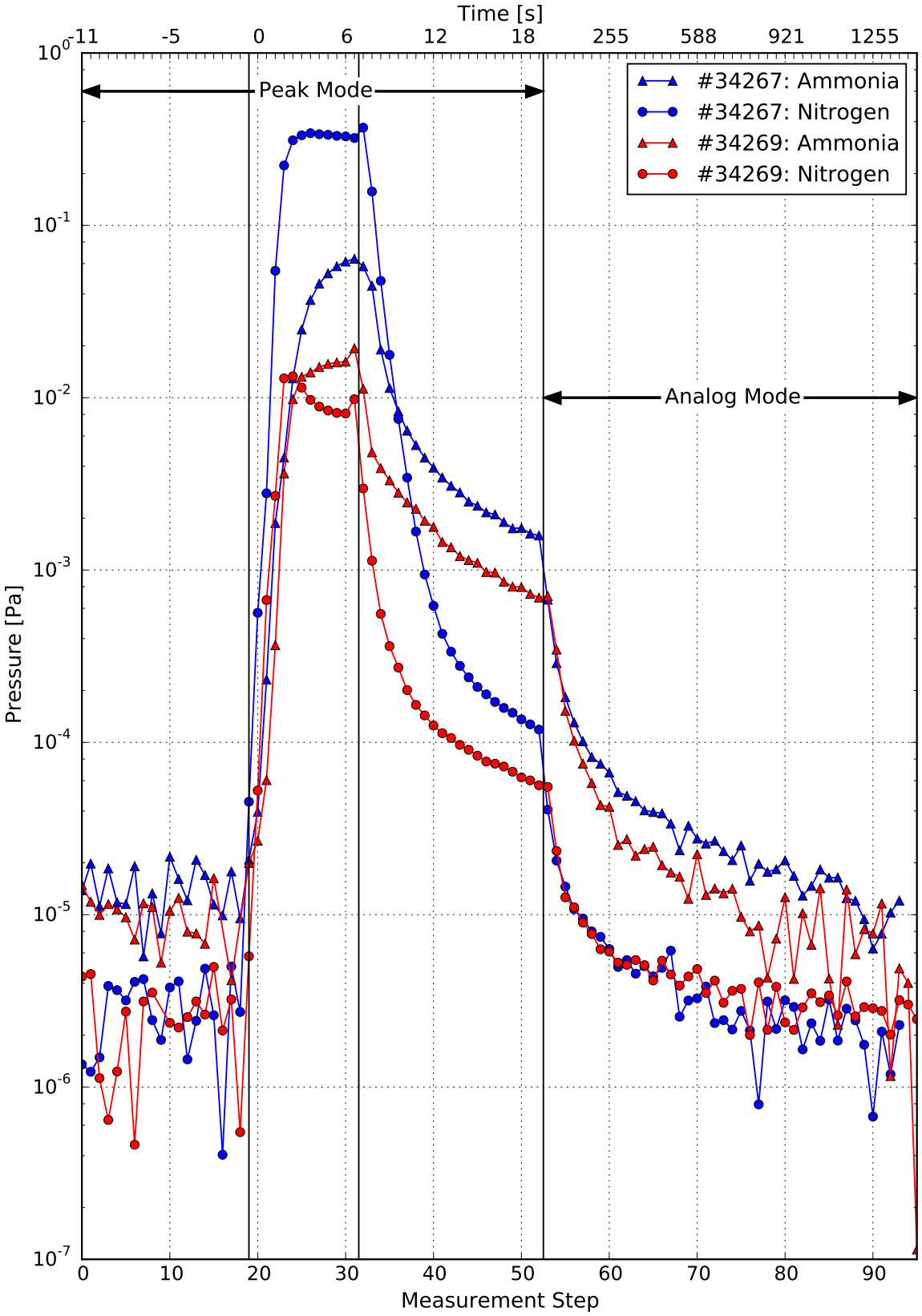

FIGURE 4.16: HPQI: Comparison of nitrogen and ammonia partial pressures during seeded discharge 34267 and legacy discharge 34269

4.5.2 Behavior of Nitrogen during Seeded and Legacy Discharges

During nitrogen seeded discharges (see figure 4.17a) a part of the puffed N_2 is pumped out directly the other part is interacting with the plasma (interacting N_2). If the nitrogen radicals go on PFCs they can be retained or recombining with stored nitrogen or hydrogen to neutral nitrogen molecules or ammonia. If these neutrals are going again to the plasma they are dissociated and ionized again or they can be pumped out directly. The sum of the directly pumped out and recombined nitrogen at the wall is then detected as the total partial pressure of N_2 with the RGA.
In contrast to seeded shots in legacy shots (see figure 4.17b) no puffing is active. Therefore the detected nitrogen and ammonia with the RGA can only come from recombinations from the wall and therefore the nitrogen intensity is not disturbed by the directly pumped out nitrogen.

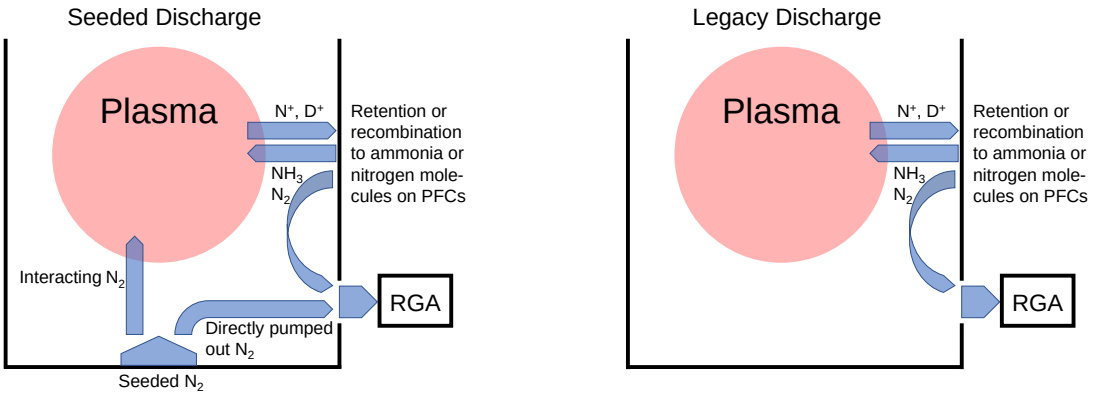

(a) Schematic of nitrogen behavior during a seeded discharge with puffed nitrogen

(b) Schematic of nitrogen behavior during a legacy discharge with retained N_2 on PFCs

FIGURE 4.17: Schematic of nitrogen behavior during a seeded and legacy discharge

4.5.3 Integrated Partial Pressures and Calculation of Correlation Factor

In this section the integrated nitrogen and ammonia signals are listed for all 16 evaluated discharges and the devices HPQI (sector 8, inner divertor) and HPQO (sector 13, outer divertor). The errors are around 10% and are caused by uncertainties of the fitting routine and the calibrations. Out of the integrated signals the correlation factors were calculated. The legacy discharges 34162, 34163, 34269, 34270, 34533 and 34535 are marked in cyan.

HPQI

In table 4.5 the integrated intensities of nitrogen and ammonia and the corresponding correlation factors can be seen. The mean value of the correlation factor for all legacy discharges is 1.87 ± 0.26.

Shotnumber	Integrated N_2 [Pa·s]	Integrated NH_3 [Pa·s]	Correlation Factor
34156	0.2551 ± 0.0140	0.0664 ± 0.0045	0.2603 ± 0.0226
34157	0.0779 ± 0.0043	0.0363 ± 0.0024	0.4660 ± 0.0404
34158	0.0711 ± 0.0039	0.0329 ± 0.0022	0.4627 ± 0.0401
34159	0.0774 ± 0.0043	0.0382 ± 0.0026	0.4935 ± 0.0428
34160	0.1201 ± 0.0066	0.0662 ± 0.0044	0.5512 ± 0.0478
34162	0.0013 ± 0.0001	0.0026 ± 0.0002	1.9934 ± 0.1728
34163	0.0068 ± 0.0004	0.0100 ± 0.0007	1.4706 ± 0.1275
34264	0.6518 ± 0.0359	0.0588 ± 0.0039	0.0902 ± 0.0078
34265	1.1343 ± 0.0624	0.1698 ± 0.0114	0.1497 ± 0.0130
34266	2.3604 ± 0.1298	0.3772 ± 0.0253	0.1598 ± 0.0139
34267	2.0919 ± 0.1151	0.4102 ± 0.0275	0.1961 ± 0.0170
34269	0.0609 ± 0.0033	0.1383 ± 0.0093	2.2709 ± 0.1969
34270	0.0200 ± 0.0011	0.0362 ± 0.0024	1.8100 ± 0.1569
34532	0.8231 ± 0.0453	0.0385 ± 0.0026	0.0468 ± 0.0041
34533	0.0220 ± 0.0012	0.0406 ± 0.0027	1.8455 ± 0.1600
34535	0.0139 ± 0.0008	0.0256 ± 0.0017	1.8417 ± 0.1596

TABLE 4.5: HPQI: Integrated nitrogen and ammonia signal and calculated correlation factors for all evaluated discharges; legacy shots are highlighted with cyan.

HPQO

The same procedure can be done for HPQO. The resulting mean correlation factor is 0.52 ± 0.11.

Shotnumber	Integrated N_2 [$\cdot 10^{-2}$ Pa·s]	Integrated NH_3 [$\cdot 10^{-2}$ Pa·s]	Correlation Factor
34156	4.8826 ± 0.2685	0.0516 ± 0.0035	0.0106 ± 0.0009
34157	2.8141 ± 0.1548	0.0338 ± 0.0023	0.0120 ± 0.0010
34158	1.7487 ± 0.0962	0.0221 ± 0.0015	0.0126 ± 0.0011
34159	2.0162 ± 0.1109	0.0220 ± 0.0015	0.0109 ± 0.0009
34160	4.7085 ± 0.2590	0.0962 ± 0.0064	0.0204 ± 0.0018
34162	0.0129 ± 0.0007	0.0068 ± 0.0005	0.5271 ± 0.0457
34163	0.0471 ± 0.0026	0.0262 ± 0.0018	0.5563 ± 0.0482
34264	2.9819 ± 0.1640	0.0494 ± 0.0033	0.0166 ± 0.0014
34265	4.3177 ± 0.2375	0.1263 ± 0.0085	0.0293 ± 0.0025
34266	9.2453 ± 0.5085	0.6876 ± 0.0461	0.0744 ± 0.0064
34267	9.0733 ± 0.4990	0.9173 ± 0.0615	0.1011 ± 0.0088
34269	0.2588 ± 0.0142	0.1475 ± 0.0099	0.5699 ± 0.0494
34270	0.1501 ± 0.0083	0.0994 ± 0.0067	0.6622 ± 0.0574
34532	0.4016 ± 0.0221	0.0209 ± 0.0014	0.0520 ± 0.0045
34533	0.0336 ± 0.0018	0.0134 ± 0.0009	0.3988 ± 0.0346
34535	0.0255 ± 0.0014	0.0098 ± 0.0007	0.3843 ± 0.0333

TABLE 4.6: HPQO: Integrated nitrogen and ammonia signal and calculated correlation factors for all evaluated discharges; legacy shots are highlighted with cyan.

4.5.4 Differences and Properties of HPQI and HPQO

By having a more detailed look on the calculated correlation factors differences and properties can be seen. Firstly the mean correlation factors between the two devices HPQI and HPQO are different by a factor of 3.6. The divertor setup is different and the cryo pump in the outer divertor is playing an additional role (see figure 4.18). The LN_2 shield of the cryo pump is removing ammonia already effectively, while nitrogen is only removed by the LHe panel, from the residual gas before it reaches HPQO. Therefore the measured ammonia intensity is effected crucially and the resulting correlation factors have to be much smaller than for HPQI, where no cryo pump is installed and the gas mixture is not affected by the different freezing temperatures with help of the cryo pump (see appendix D).

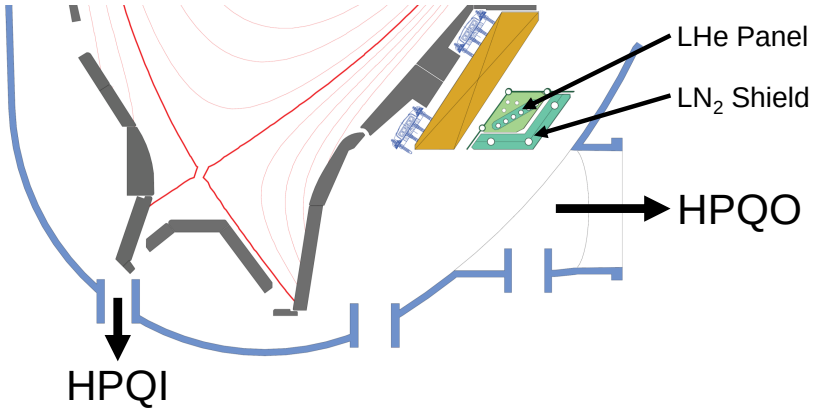

FIGURE 4.18: Divertor setup with cryo pump location

Secondly by comparing the correlation factor of the first seeded discharge of each set one can see large differences: for HPQI the correlation factors for discharges 34156, 34264 and 34532 are 0.260, 0.090 respectively 0.047. By having a closer look to the valves used for seeding (see table 4.1, 4.2 and 4.3) during the first set valve Du09X was not used which is next to the RGA HPQI. By applying the local seeding effect already discussed before the huge difference in the correlation factor can be explained by this effect. If nitrogen is not puffed at the same location as the RGA is installed the measured nitrogen is much smaller and therefore the correlation factor increases. This can also be seen for the data of HPQO: the correlation factors of the first discharge of each set are: 0.011, 0.017 and 0.052. Nitrogen was seeded in sector 13 for the first two, so the correlation factor is small, while for the latter one valve Du13X was not used and the corresponding nitrogen intensity is smaller.

Thirdly during all sets of discharges the correlation factor is increasing. This indicates a build up of the retained nitrogen in the vessel during consecutive seeded discharges. Because in the second seeded discharge not only puffed nitrogen is forming ammonia but also retained nitrogen this correlation factor is a superposition of both processes. Additionally a saturation of the correlation factor can be seen (see figure 4.19). This saturation was already seen in different analysis before [25].

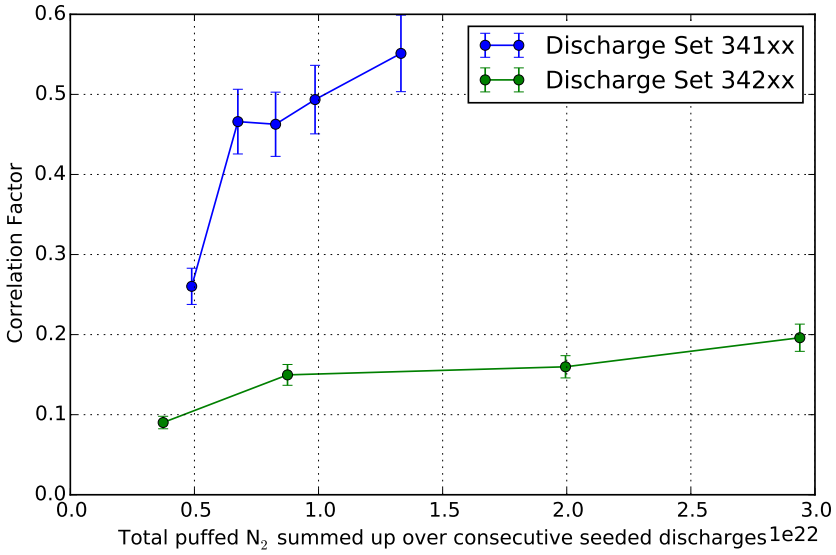

FIGURE 4.19: HPQI: Saturation of correlation factor for consecutive seeded discharges.

4.5.5 Calculation of the Nitrogen Content in the Plasma

The mean correlation factor describes in the model the correlation between ammonia and nitrogen if all of the nitrogen had interacted with the plasma. By applying it to the measured intensity of ammonia during seeded discharges the estimated nitrogen signal can be calculated which entered the plasma.
The total interacting nitrogen would be the sum of the calculated nitrogen and the nitrogen in the formed ammonia. In figure 4.20 the integrated partial pressures of nitrogen and ammonia can be seen with the reconstructed intensity of interacting nitrogen for the device HPQI. For all non-seeded discharges the reconstructed nitrogen content overlaps quite well with the measured data.
The reconstructed nitrogen signals for HPQO look similar (see figure 4.21). In comparison to HPQI the reconstructed nitrogen is larger than the measured ammonia due to the small correlation factor which is affected by the cryo pumps.
A good agreement between calculated and measured nitrogen content for non-seeded discharges is visible like in the inner divertor (HPQI).

For consecutive legacy discharges the amount of measured nitrogen and ammonia is decreasing. The legacy discharges 34162 and 34163 are an exception, which is visible for HPQI and HPQO. Because discharge 34162 was canceled already after less than 1 second the production of ammonia and nitrogen is much smaller than for discharge 34163.

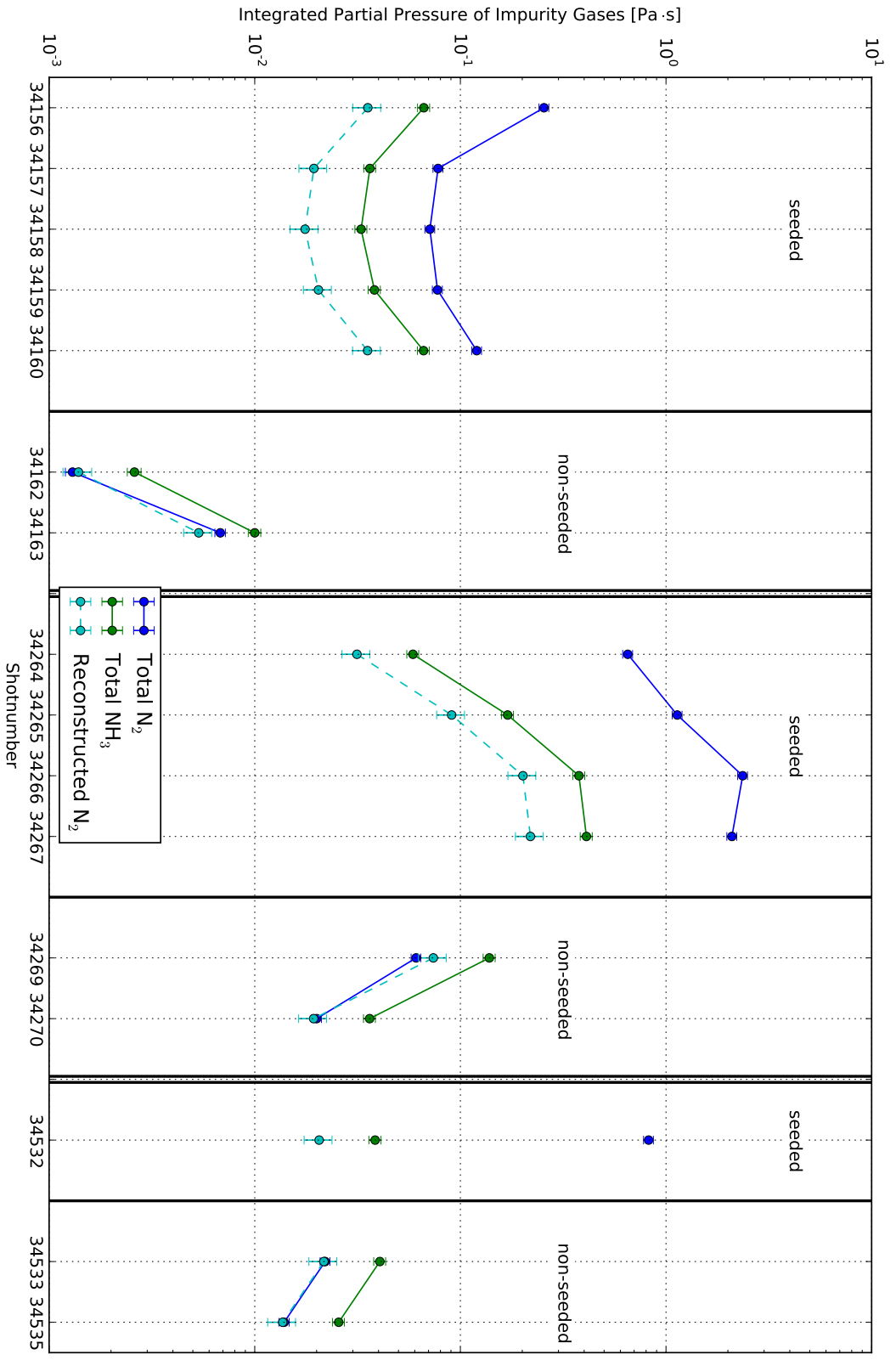

FIGURE 4.20: HPQI: Integrated partial pressures of nitrogen and ammonia and the reconstructed nitrogen

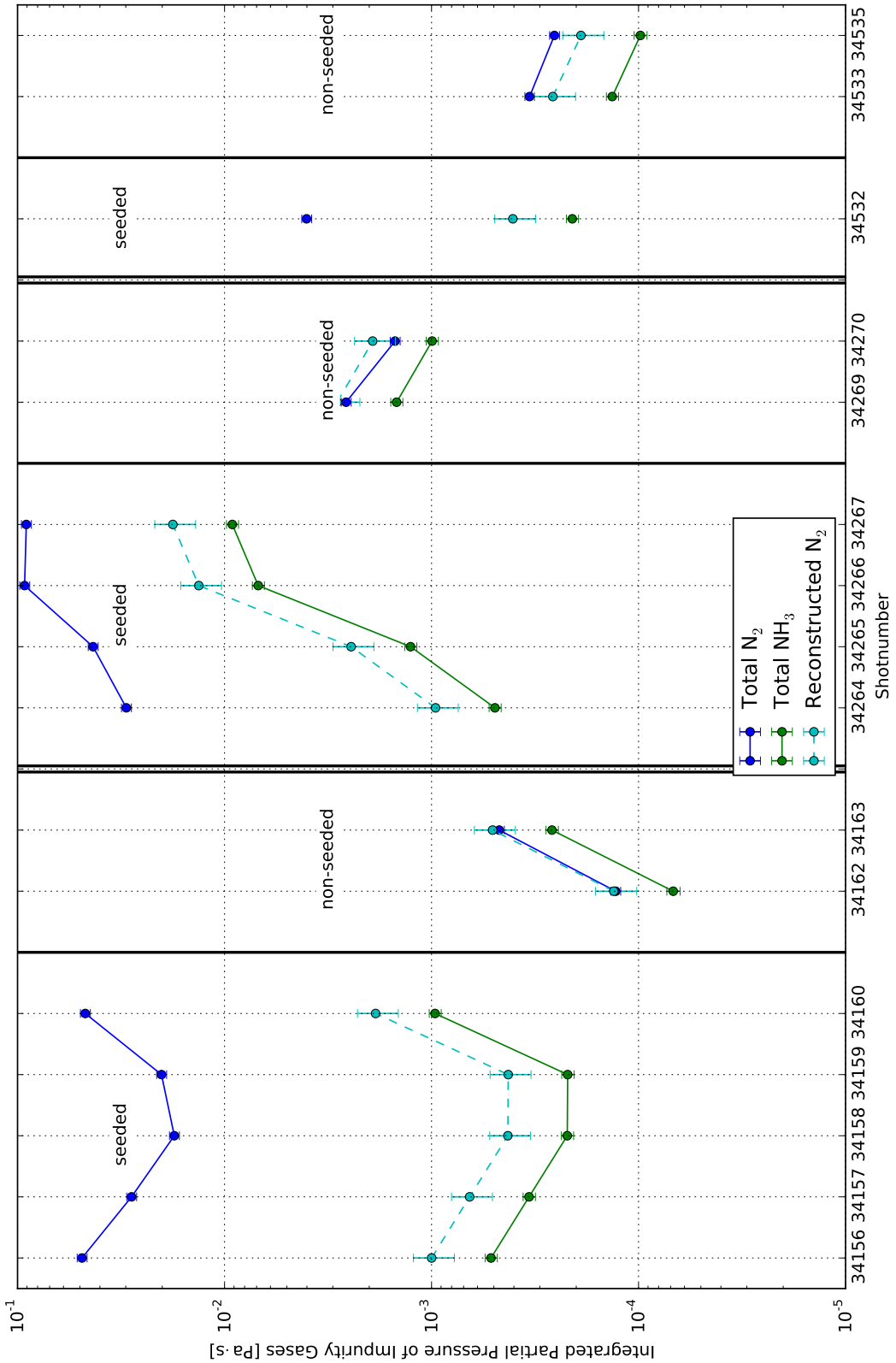

FIGURE 4.21: HPQO: Integrated partial pressures of nitrogen and ammonia and the reconstructed nitrogen

Crucial is the comparison of inner and outer divertor measurements. In table 4.7 the results of the reconstructed nitrogen signals can be seen. A

Shotnumber	Reconstructed N_2 HPQI [Pa·s]	Reconstructed N_2 HPQO [Pa·s]
34156	0.0355 ± 0.0055	0.0010 ± 0.0002
34157	0.0194 ± 0.0030	0.0007 ± 0.0001
34158	0.0176 ± 0.0027	0.0004 ± 0.0001
34159	0.0204 ± 0.0032	0.0004 ± 0.0001
34160	0.0354 ± 0.0055	0.0019 ± 0.0004
34264	0.0314 ± 0.0048	0.0010 ± 0.0002
34265	0.0907 ± 0.0014	0.0024 ± 0.0005
34266	0.2015 ± 0.0031	0.0133 ± 0.0029
34267	0.2191 ± 0.0034	0.0178 ± 0.0039
34532	0.0206 ± 0.0032	0.0004 ± 0.0001

TABLE 4.7: Reconstructed nitrogen signals for HPQI and HPQO for all seeded discharges

clear discrepancy is visible between both devices. The reconstructed nitrogen intensity of HPQI is roughly by a factor of 30 higher compared to the intensity for the outer divertor. Nitrogen and ammonia are pumped by the cryo pump with different degrees of effectiveness and therefore the correlation factor for non-seeded discharges is disturbed. This leads to a wrong interpretation of the the reconstructed nitrogen from the outer divertor data due to the unknown effect of the cryo pump.
Because of that it seems that the acquired data from the inner divertor seems to be more trustworthy. The nitrogen content in the plasma during the discharge is the sum of the reconstructed nitrogen and the ammonia integrated pressures. Because the ratio is given by the correlation factor which is 1.87 for the device HPQI it yields that about 50% of the interacting nitrogen atoms are converted into ammonia during the discharge while the other half is recombining to nitrogen molecules.

4.5.6 Conclusion

It's possible to gain the nitrogen content out of the ammonia signals by RGAs with the help of the correlation factor. But this has also difficulties like the positions of the RGAs, the puffing locations, especially in the outer divertor, where the cryo pump is disturbing the measurements. Data analysis of the warming up process of the cryo pump suggests that a large amount of ammonia is frozen onto the LN_2 shield and therefore disturbs the residual gas composition (see appendix D). Due to that the nitrogen content in the plasma can be reconstructed only with the data of the RGA in the inner divertor

where the cryo pump is not disturbing the gas mixture, nitrogen and ammonia content.
A tube at the outer divertor was installed which allows to pump residual gas to the outer RGA so that the gas won't be influenced by the cryo pump. Therefore it will be possible to verify the measurements in the inner divertor in the next campaign and get a more detailed view on the residual gas mixture.
The data suggest that around 50% of the interacting nitrogen atoms are converted to ammonia. The sum of reconstructed N_2 and detected ammonia leads then to the total amount of interacted nitrogen. If the total seeded nitrogen is compared to the detected ammonia the formation ratio is around 5% which already could be showed [9].
With the help of RGAs no distinction of the kind of nitrogen retention (as nitrides or ammonia) is possible. Therefore other models are needed.

Chapter 5

Conclusion and Outlook

5.1 Conclusion

During this master thesis the nitrogen content in the divertor plasma during seeded discharges was investigated. Therefore quadrupole mass spectrometers were used as main diagnostic to analyze the residual gas of 16 nitrogen seeded and legacy discharges. In ASDEX Upgrade several mass spectrometers are used to measure the residual gas mixture at different locations of the fusion research device. For the deconvolution of the measured mass-to-charge spectra the model of Price and Iglesia was used for the description of the cracking patterns of the main impurities in the residual gas. Afterwards a minimization procedure approach of A. Drenik [23] was used to determine the partial pressures of each impurity gas separately.

During a more detailed look on the acquired data a local effect of seeding could be seen in the RGA and pressure data. Because a significant amount of seeded nitrogen and/or deuterium is not ionized and does not interact with the plasma it is pumped out near the seeding location. Therefore the intensity of measured nitrogen in the mass spectrometers is dependent on the seeding location. This phenomena is also visible in the pressure measurements of different baratrons for different usages of seeding valves. In the comparison of evaluated discharges the total pressure is dropping by a factor of two and the nitrogen intensity of the corresponding RGA by a factor of six if there is no seeding next to the measurement location. This local effect could be avoided by analyzing the created ammonia during seeded discharges. Consequently it can be assumed that if the seeded atoms become ionized, their toroidal transport is enhanced and a symmetrical behavior is observable.

The local puffing effect and the comparison of the RGA signals with CXRS impurity signals suggest that ammonia is an appropriate indicator for N_2 in the plasma. To assess the nitrogen enrichment in the divertor plasma the correlation between nitrogen and ammonia signal for discharges was used. The large difference of the correlation factors during legacy discharges for the in-

ner and outer divertor relate to the different pumping speeds of ammonia and nitrogen of the cryo pump. Because of the change of the gas mixture due to the cryo pump the predictions based on the outer divertor data are strongly affected. By the reconstruction of the nitrogen signal which interacted with the plasma the total amount of nitrogen can be gained by the sum of the reconstructed nitrogen and the calculated ammonia. The comparison of the sum of those signals with the total measured nitrogen signal imply that only a very small fraction of the seeded nitrogen is interacting with the plasma and leads to cooling of the plasma. The data leads to a conversion of around 5% of the seeded nitrogen to ammonia (see also [9]), while around 50% of the interacting nitrogen are converted to ammonia. If the seeding would be more effective a even higher amount of ammonia would be produced which can lead to further implications on the gas plant of ITER if nitrogen is used as extrinsic radiator for divertor cooling.

5.2 Outlook

The calibration procedure showed that a frequent calibration of the main impurity gases lead to good fitting results. For a more detailed residual gas analysis the calibration procedure should be frequently repeated.
Additionally a more realistic approach for calibration would be the calibration with a gas mixture where deuterium would be the main part of the gas and the impurity gases like nitrogen or methane are only a component of the total gas mixture in the percentage area.

To understand the impact of the seeding location on the amount of produced ammonia and the local measurement effects other locations for nitrogen puffing can be used like from the top or the midplane. The same level of heat load control and confinement enhancement could be achieved at lower divertor N_2 pressures and ammonia formation rates.

Appendix A

Cracking Pattern Matrices $\mathcal{A}$

$$\mathcal{A}^{H_2O} = \begin{pmatrix} 0 & 0 & 0 \\ 0 & 0 & 0 \\ 0 & 0 & 0 \\ 0 & 0 & 0 \\ 0 & 0 & 1 \\ 0 & w_0 + \frac{w_1}{2} & 0 \\ w_0 & \frac{w_1}{2} + w_2 & 0 \\ w_1 & 0 & 0 \\ w_2 & 0 & 0 \end{pmatrix} \tag{A.1}$$

$$\mathcal{A}^{NH_3} = \begin{pmatrix} 0 & 0 & 0 & 0 \\ 0 & 0 & 0 & 0 \\ 0 & 0 & 0 & 1 \\ 0 & 0 & w_0 + \frac{2w_1}{3} + \frac{w_2}{3} & 0 \\ 0 & w_0 + \frac{w_1}{3} & \frac{w_1}{3} + \frac{2w_2}{3} + w_3 & 0 \\ w_0 & w_0 + \frac{2w_1}{3} + \frac{2w_2}{3} & 0 & 0 \\ w_1 & \frac{w_2}{3} + w_3 & 0 & 0 \\ w_2 & 0 & 0 & 0 \\ w_3 & 0 & 0 & 0 \end{pmatrix} \tag{A.2}$$

$$\mathcal{A}^{CH_4} = \begin{pmatrix} 0 & 0 & 0 & 0 & 1 \\ 0 & 0 & 0 & w_0 + \frac{3w_1}{4} + \frac{w_2}{2} + \frac{w_3}{4} & 0 \\ 0 & 0 & w_0 + \frac{w_1}{2} + \frac{w_2}{6} & \frac{w_1}{4} + \frac{w_2}{2} + \frac{3w_3}{4} + w_4 & 0 \\ 0 & w_0 + \frac{w_1}{4} & \frac{w_1}{2} + \frac{2w_2}{3} + \frac{w_3}{2} & 0 & 0 \\ w_0 & \frac{3w_1}{4} + \frac{w_2}{2} & \frac{w_2}{6} + \frac{w_3}{2} + w_4 & 0 & 0 \\ w_1 & \frac{w_2}{2} + \frac{3w_3}{4} & 0 & 0 & 0 \\ w_2 & \frac{w_3}{4} + w_4 & 0 & 0 & 0 \\ w_3 & 0 & 0 & 0 & 0 \\ w_4 & 0 & 0 & 0 & 0 \end{pmatrix} \tag{A.3}$$

Appendix B

Positions of Pressure Gauges and Mass Spectrometers in ASDEX Upgrade

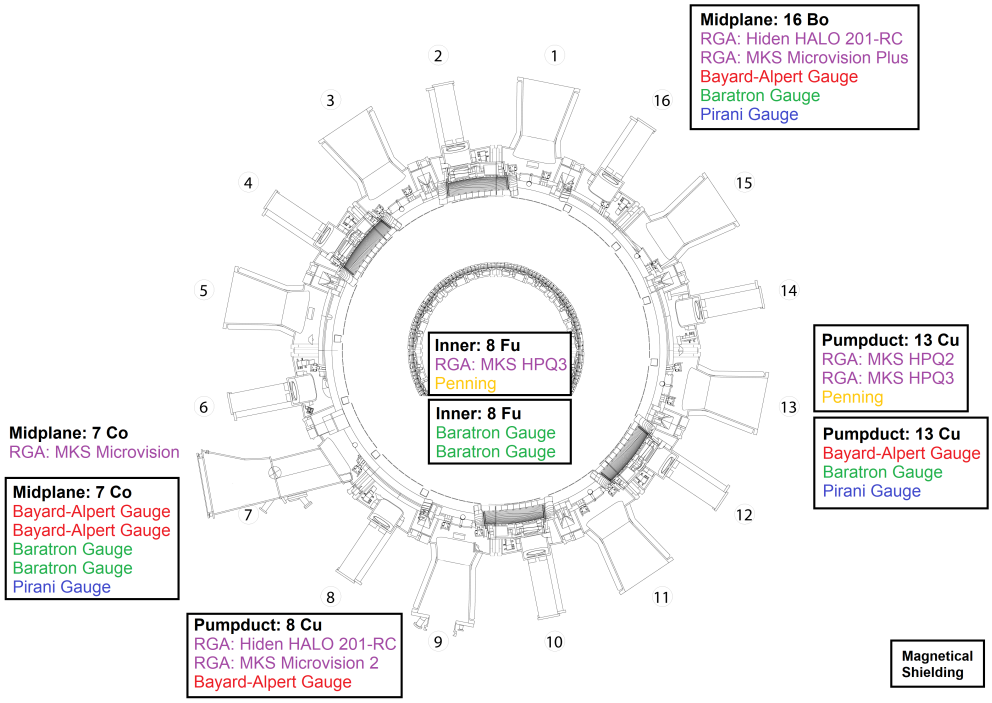

FIGURE B.1: Positions of residual gas analysers and pressure gauges.

Appendix C

Fragmentation Vectors of Calibrations for all used Devices

	D_2	N_2	CH_4	H_2O	NH_3
HPQI	5575 ± 558	2380 ± 131	1714 ± 178	2900 ± 580	2549 ± 171
HPQO	750	183 ± 18	130 ± 13	215 ± 22	189 ± 19
HPQO2	2474	618	1010	-	-
MV	550661	323224	243861	-	-
HIDEN2	55845	58535	-	-	-

Table C.1: Calibration Factors of all MSPs [Pa]

	D_2	N_2	CH_4	H_2O	NH_3
HPQI	$(1, 0.007)^T$	$(1, 0.055, 0.007)^T$	$(1, 0.826, 0.109, 0.050, 0.016)^T$	$(1, 0.300, 0.100)^T$	$(1, 0.630, 0.034, 0.000)^T$
HPQO	$(1, 0.012)^T$	$(1, 0.068, 0.007)^T$	$(1, 0.855, 0.152, 0.071, 0.022)^T$	$(1, 0.260, 0.070)^T$	$(1, 0.790, 0.039, 0.000)^T$
HPQO2	$(1, 0.004)^T$	$(1, 0.150, 0.007)^T$	$(1, 0.866, 0.293, 0.149, 0.050)^T$	$(1, 0.460, 0.160)^T$	-
MV	$(1, 0.006)^T$	$(1, 0.058, 0.007)^T$	$(1, 0.795, 0.103, 0.044, 0.013)^T$	$(1, 0.320, 0.100)^T$	-
HIDEN2	$(1, 0.011)^T$	$(1, 0.043, 0.000)^T$	-	-	-

Table C.2: Fragmentation Vectors of all MSPs for small pressures

Appendix D

Cryo Warm-up Measurements of HPQI

After the last discharge of a week the cryo pump is regenerated by heating the LHe panel and the LN_2 shield up and release the trapped gases. In figure D.2 the regeneration of the cryo pump was recorded by HPQI during heating up at the 2017-06-08. After heating up the LHe panel nitrogen is released which has the lowest boiling point of the main residual gases (see D.1). The release can be seen during the measurement steps 100 and 115. After the heating up of the LHe panel the LN_2 is heated up. Between step 125 and 150 methane is the next main residual gas which is released. After that ammonia is released from the LN_2 shield surface. The partial pressure for ammonia rises during that time with a factor of up to 10. Water stays roughly constant at the background pressure during the whole measurement.

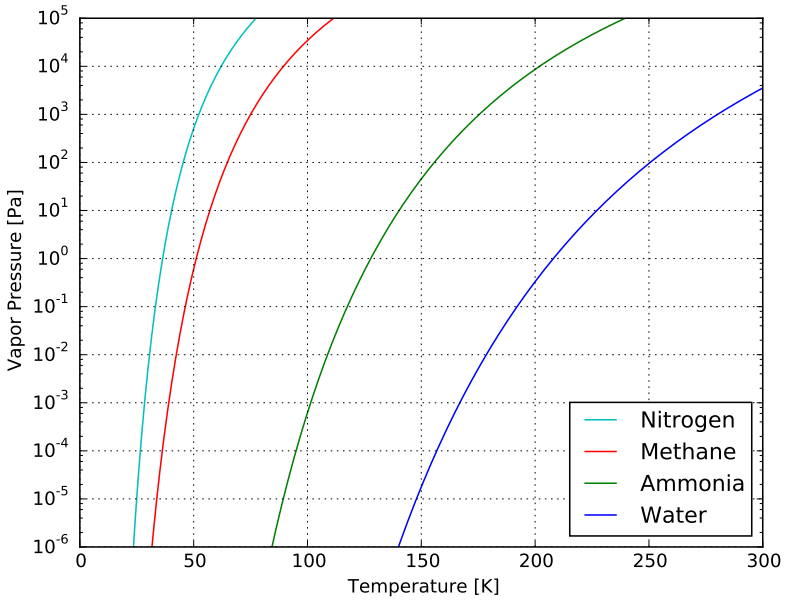

FIGURE D.1: Vapor pressure curves for the main impurities in ASDEX Upgrade

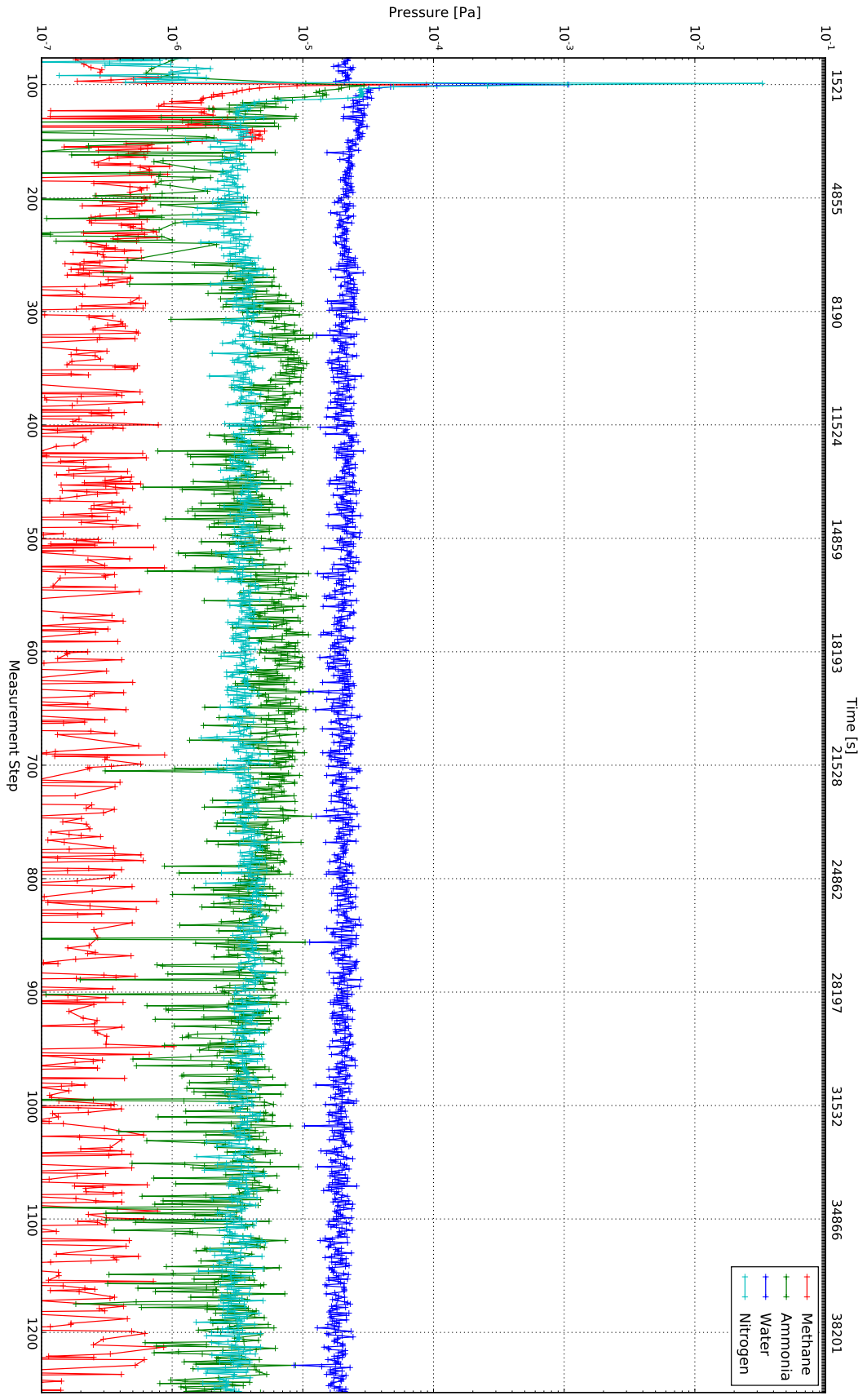

FIGURE D.2: HPQI: Partial pressures of residual gases during cryo warm-up of the 2017-06-08

Bibliography

[1] Eurostat. Electricity and Heat Statistics. http://ec.europa.eu/eurostat/statistics-explained/index.php/Electricity_and_heat_statistics, 2017. [Online, from 20. December 2017].

[2] S. Atzeni and J. Mayer ter Vehn. *The Physics of Inertial Fusion*. Oxford University Press, 2004.

[3] Wikipedia. Nuclear Fusion. https://en.wikipedia.org/wiki/Nuclear_fusion. [Online, from 07. February 2018].

[4] Naval Research Laboratory. NRL Plasma Formulary, 2016.

[5] J. Wesson. *Tokamaks*. Oxford University Press, 3rd edition, 2004.

[6] ASDEX Upgrade. Drawing Gallery. http://www.aug.ipp.mpg.de/aug/local/aug_only/AUG_Aufbau/Drawing_Gallery/. [Online, from 07. February 2018].

[7] A. Drenik et al. Evolution of nitrogen concentration and ammonia production in N_2-seeded H-mode discharges at AUG. *Not Yet Published*.

[8] M. Oberkofler et al. Nitrogen retention mechanisms in tokamaks with beryllium and tungsten plasma-facing surfaces. *Physica Scripta*, 2016(T167):014077, 2016.

[9] D. Neuwirth. Formation of ammonia during nitrogen seeded discharges at the Tokamak ASDEX Upgrade, 2012.

[10] V. Rohde and M. Oberkofler. Ammonia production in nitrogen seeded plasma discharges in ASDEX Upgrade. *Journal of Nuclear Materials*, 463:672–675, 2015.

[11] A. Kallenbach et al. Divertor power load feedback with nitrogen seeding in ASDEX Upgrade. *Plasma Physics and Controlled Fusion*, 52(055002), 2010.

[12] A. Kallenbach. The ASDEX Upgrade tokamak. http://www.aug.ipp.mpg.de/augtwiki/bin/viewfile/AUG/TopicRemarks_GuidelinesForNewcomers?rev=1;filename=AUG-description_Sept2016.pdf. [Online, from 07. February 2018].

[13] V. Rohde et al. Dynamic and static deuterium inventory in ASDEX Upgrade with tungsten first wall. *Nuclear Fusion*, 49(8):085031, 2009.

[14] MKS Instruments. Baratron Capacitance Manometers. `https://www.mksinst.com/docs/ur/barainfo1.aspx`. [Online, from 08. February 2018].

[15] J. Throck Watson and O.David Sparkman. *Introduction to Mass Spectrometry*. John Wiley and Sons, Ltd, 4th edition, 2007.

[16] MKS Instruments. HPQ3/HPQ3S - Data Sheet. `https://www.mksinst.com/docs/UR/HPQ3-DS.pdf`. [Online, from 08. February 2018].

[17] Hiden Analytical. Hiden Analytical - RGA Data Sheet. `http://www.hidenanalytical.com/wp-content/uploads/2017/02/TDS-188-3_RGA_Catalogue.pdf`. [Online, from 08. February 2018].

[18] MKS Instruments. Microvision 2 - Data Sheet. `https://www.mksinst.com/docs/UR/MicroVision2ds.pdf`. [Online, from 08. February 2018].

[19] Bond Dissociation Energies. `https://labs.chem.ucsb.edu/zakarian/armen/11---bonddissociationenergy.pdf`, 2017. [Online, from 09. November 2017].

[20] G. L. Price and E. Iglesia. Matrix Method for Correction of Mass Spectra in Deuterium-Exchange Applications. *Industrial & Engineering Chemistry Research*, 28(6):839–844, 1989.

[21] D. H. Lenz and Jr. WM. C. Conner. Computer analysis of the cracking patterns of deuterated hydrocarbons. *Analytica Chimica Acta*, 173:227 – 238, 1985.

[22] F. Reimold. Praktikumsbericht: Massenspektroskopie am ASDEX Upgrade.

[23] A. Drenik et al. Detection of ammonia by residual gas analysis in AUG and JET. *Fusion Engineering and Design*, 124:239–243, 2017. Proceedings of the 29th Symposium on Fusion Technology (SOFT-29) Prague, Czech Republic, September 5-9, 2016.

[24] S. Potzel et al. Formation of the high density front in the inner far SOL at ASDEX Upgrade and JET. *Journal of Nuclear Materials*, 463:541–545, 2015.

[25] M. Oberkofler et al. Plasma-wall interactions with nitrogen seeding in all-metal fusion devices: Formation of nitrides and ammonia. *Fusion Engineering and Design*, 98 - 99:1371 – 1374, 2015. Proceedings of the 28th Symposium On Fusion Technology (SOFT-28).

Affirmation

I hereby certify that for this thesis I have worked independently and used no other than the specified sources, references and resources.

Garching, the

Thomas Reichbauer

Danksagung

Ich möchte mich hier bei allen bedanken, die mich während der Forschungsphase und der Masterarbeit unterstützt haben.

Mein besonderer Dank gilt Volker Rohde, der immer versucht hat sich Zeit für meine Fragen und Probleme zu nehmen, ob technisch, physikalisch oder in der wissenschaftlichen Formulierung von Texten und diese Masterarbeit erst möglich gemacht hat. Ein weiterer besonderer Dank geht an Aleksander Drenik, mit dem ich stundenlang Probleme zur Datenauswertung diskutieren konnte, der mich immer wieder auf neue Ideen gebracht hat und mit dem ich vor allem über ein Jahr in der Datenauswertung der Massenspektroskopie am ASDEX Upgrade arbeiten durfte.

Ich möchte auch meinen Bürokollegen Klara Höfler, Alexander Bauer und Johannes Illerhaus für die vielen lustigen Momente, unseren eigenen "Projekten" und viele interessante Diskussionen Danke sagen.
Ein besonderer Dank gilt Klara Höfler, die mir immer mit Rat und Tat zur Seite stand, sei es beim Debuggen von Code, der Postergestaltung für die DPG Erlangen und auch einen tieferen Einblick in das Core-Plasma selbst.
Zudem möchte ich mich bei Johannes Illerhaus und Lennart Bock für den regelmäßigen Kaffeenachschub bedanken. Für schnelle Hilfe bei Problemen zum System, technischen und physikalischen Fragen möchte ich mich bei Stephan Glöggler, Dominik Brida, Lennart Bock, Felician Mink und Gregor Birkenmeier bedanken.

Ein weiterer Dank geht an das ganze ASDEX Upgrade Team, das den laufenden Betrieb und die Experiemente ermöglicht und mich so mit vielen Daten für die Analyse eingedeckt haben. Insbesondere möchte ich mich bei Rachael McDermott bedanken, die sich viel Zeit genommen hat um die Verunreinigungsanalyse im Core-Plasma mit Hilfe der CXRS Daten auszuwerten.

Zu Schluss gilt mein größter Dank meiner Familie, die mich auf meinem Lebensweg immer unterstützt hat und mir die Möglichkeit gegeben hat meine Interessen an der Physik zu verfolgen.

Vielen herzlichen Dank!
Thank you very much!
Najlepša hvala!

"The more often you look at diagnostic signals the less you trust them."
Aleksander Drenik